# Acetylcholine Modulates the Precision of Prediction Error in the Auditory Cortex

***David Pérez-González[†1,2,3], Ana B. Lao-Rodríguez[†1,2], Cristian Aedo-Sánchez[1,2] & Manuel S. Malmierca[1,2,4*]***

[1] Cognitive and Auditory Neuroscience Laboratory, Institute of Neuroscience of Castilla y León, Calle Pintor Fernando Gallego 1, 37007 Salamanca, Spain

[2] Institute for Biomedical Research of Salamanca (IBSAL), 37007 Salamanca, Spain.

[3] Department of Basic Psychology, Psychobiology and Behavioural Science Methodology, Faculty of Psychology, Campus Ciudad Jardín, University of Salamanca, 37005 Salamanca, Spain

[4] Department of Biology and Pathology, Faculty of Medicine, Campus Miguel de Unamuno, University of Salamanca, 37007 Salamanca, Spain

† These authors contributed equally to this work

* Corresponding and leading author: msm@usal.es

## ABSTRACT

A fundamental property of sensory systems is their ability to detect novel stimuli in the ambient environment. The auditory brain contains neurons that decrease their response to repetitive sounds but increase their firing rate to novel or deviant stimuli; the difference between both responses is known as stimulus-specific adaptation or neuronal mismatch (nMM). Here, we tested the effect of microiontophoretic applications of ACh on the neuronal responses in the auditory cortex (AC) of anesthetized rats during an auditory oddball paradigm, including cascade controls. Results indicate that ACh modulates the nMM, affecting prediction error responses but not repetition suppression, and this effect is manifested predominantly in infragranular cortical layers. The differential effect of ACh on responses to standards, relative to deviants (in terms of averages and variances), were consistent with the representational sharpening that accompanies an increase in the precision of prediction errors. These findings suggest that ACh plays an important role in modulating prediction error signaling in the AC and gating the access of these signals to higher cognitive levels.

## INTRODUCTION

Neuromodulation strongly impacts sensory processing by influencing neuronal excitability or synaptic processes in neuronal circuits (Hasselmo and Giocomo, 2006; Lucas-Meunier et al., 2003; Metherate, 2011; Muñoz and Rudy, 2014; Picciotto et al., 2012). Acetylcholine (ACh) is a widely distributed neuromodulator throughout the brain, including the auditory cortex (AC), and modulates processes such as attention, learning, memory, arousal, sleep and/or cognitive reinforcement (Batista-Brito et al., 2018; Dalley et al., 2004; Franklin and Frank, 2015). The main source of ACh to the AC is the basal forebrain (Chavez and Zaborszky, 2017; Mesulam, 2013; Zaborszky et al., 2008). In the auditory system, cholinergic modulation is known to alter frequency response areas generating changes across frequency tuning, decreasing the acoustic threshold at the characteristic frequency, and changing the encoding of the spectral representation of many auditory neurons (Ma and Suga, 2005; Metherate, 2011) Thus, ACh promotes neuronal and synaptic plasticity at different temporal scales (Kamke et al., 2005; Kilgard and Merzenich, 1998).

Here, we characterized the effect of ACh on stimulus-specific adaptation (SSA), a type of neuronal adaptation found in the AC. SSA is elicited by an oddball paradigm, which comprises a pattern of repeating sounds (standards), interrupted by a low-probability and unexpected sound (deviant). The deviant usually differs in frequency, but could differ on any other physical dimension from the standard sound, or otherwise violate a pattern of regularity established by the standard (Chen et al., 2015; Nieto-Diego and Malmierca, 2016; Parras et al., 2017; Ulanovsky et al., 2003; von der Behrens et al., 2009).

Thus, neurons that exhibit SSA adapt specifically to the standard stimulus but resume their firing when a deviant stimulus appears. SSA has been proposed to be a neuronal correlate of 'mismatch negativity' (MMN), an evoked potential obtained in human and animal electroencephalographic studies using the oddball paradigm (Nieto-Diego and Malmierca, 2016; Ulanovsky et al., 2003). Hence, SSA has been also referred to as neuronal mismatch (nMM) in animal models (Casado-Román et al., 2020; Lao-Rodríguez et al., 2023; Parras et al., 2020, 2017), a nomenclature that highlights deviance detection, as well as other underlying processes other than neuronal adaptation. Because nMM is considered a form of short-term plasticity (Ogawa and Oka, 2015) and ACh has been shown to play a role in this type of neural plasticity (Marshall et al., 2016; Moran et al., 2013; Parr and Friston, 2017; Vossel et al., 2012) it is plausible that ACh may be involved in the generation and/or modulation of nMM. Furthermore, it has been shown that ACh differentially modulates the neural response to the standard stimulus in neurons of the IC (Ayala and Malmierca, 2015).

Currently, MMN and nMM are best explained by the predictive coding theory (Friston, 2008, 2005). According to the predictive coding framework, higher-level cortical areas generate predictions about sensory streams that are conveyed in a top-down manner to lower hierarchical levels, to suppress the ascending neuronal activity evoked by sensory events that can be anticipated. However, when current predictions do not match the sensory inputs, the lower levels then send forward bottom-up prediction errors to higher hierarchical levels (Friston and Kiebel, 2009).

In the setting of an oddball paradigm, every evoked response is considered to be a prediction error response. When the stimulus does not change, sensory learning enables better predictions to progressively attenuate the response to standards until an oddball or deviant stimulus is encountered — and a large prediction error is seen. The prediction

error response to oddball stimuli may be further augmented by increasing the precision or gain of prediction errors: predictive coding models weigh sensory prediction errors by their precision, which is the inverse of variance. Precision weighting of prediction errors therefore encodes the confidence in the accuracy of the information (i.e., prediction errors) in terms of their signal-to-noise ratio (Parr and Friston, 2017). In neurobiological terms, precision has been suggested to be mediated by synaptic gain modulation; namely, the sensitivity of postsynaptic responses to neural inputs (Adams et al., 2021) and is likely implemented by cholinergic neuromodulation (Moran et al., 2013; Yu and Dayan, 2005, 2002). Increasing the gain of certain neuronal populations — e.g., superficial pyramidal cells reporting prediction errors – affords them privileged access to higher levels of processing and ensuing Bayesian belief updating. This can be likened to attentional gain in psychological terms – or increasing the Kalman gain in terms of Bayesian filtering.

According to the predictive coding model there are therefore two mechanisms underlying the MMN/nMM (Auksztulewicz and Friston, 2016; Carbajal and Malmierca, 2018; Friston, 2008; Harms et al., 2020; Parras et al., 2017). First, nMM could reflect the repetition suppression (RS) of the response to the predictable stimuli (standards) due to sensory learning – that resolves sensory prediction errors as predictions become more accurate. In addition, nMM could also reflect an increase in the precision or gain afforded prediction errors, when the (oddball) stimulus cannot be predicted; enabling the ascending prediction errors to revise higher level representations about the auditory stream. In short, oddball stimuli elicit an enhanced neural response when an unexpected (deviant) stimulus is presented. Repetition suppression and prediction error modulation can be distinguished using control sequences (Ruhnau et al., 2012), and there is now evidence in both humans and rodents that MMN/nMM receives contributions from both

110 prediction error (modulation) and repetition suppression (sensory learning) at various
111 levels of the auditory system (Ishishita et al., 2019; Parras et al., 2017).

112 The main goal of the present study was to determine the role that ACh plays in the
113 modulation of prediction errors and repetition suppression in the rat AC; utilizing
114 control sequences to disambiguate these mechanisms (Nieto-Diego and Malmierca,
115 2016; Parras et al., 2017). We used microiontophoretic injections of ACh to determine
116 how ACh neurotransmission affects the responses of AC neurons that exhibit nMM, to
117 establish the role of ACh on prediction error modulation and repetition suppression, in
118 both primary and secondary AC areas.

119

120 **RESULTS**

121 To explore the influence of cholinergic modulation on nMM, we recorded a total of 113 units
122 in the AC before, during and after the microiontophoretic injection of acetylcholine in the rat.
123 Recording depths ranged 120–1191 μm including neurons from all layers.

124 To allocate each recorded neuron to a specific field in the AC, we recorded the frequency
125 response area (FRA) and analyzed the topographical distribution of CF (characteristic
126 frequency) for each unit. Each recording was assigned to a dorsoventral and rostrocaudal
127 coordinate system relative to bregma as in previous studies (Nieto-Diego and Malmierca,
128 2016; Parras et al., 2017; Polley et al., 2007). This analysis allowed us to pool the data from
129 all animals (Fig. 1a) and construct a synthetic map of the CF across the entire rat auditory
130 cortex (Nieto-Diego and Malmierca, 2016; Parras et al., 2017). Similar to these previous
131 studies, we found a high-frequency reversal zone between ventral auditory field (VAF,
132 caudally) and anterior auditory field (AAF, rostrally), a low-frequency reversal zone between
133 A1 and posterior auditory field (PAF, dorso-caudally), and a high-frequency reversal between

VAF and supra-rhinal auditory field (SRAF, ventrally). Thus, we could reliably define the lemniscal (A1, AAF, and VAF) and non-lemniscal (SRAF, PAF) auditory cortical fields as shown in Fig. 1b.

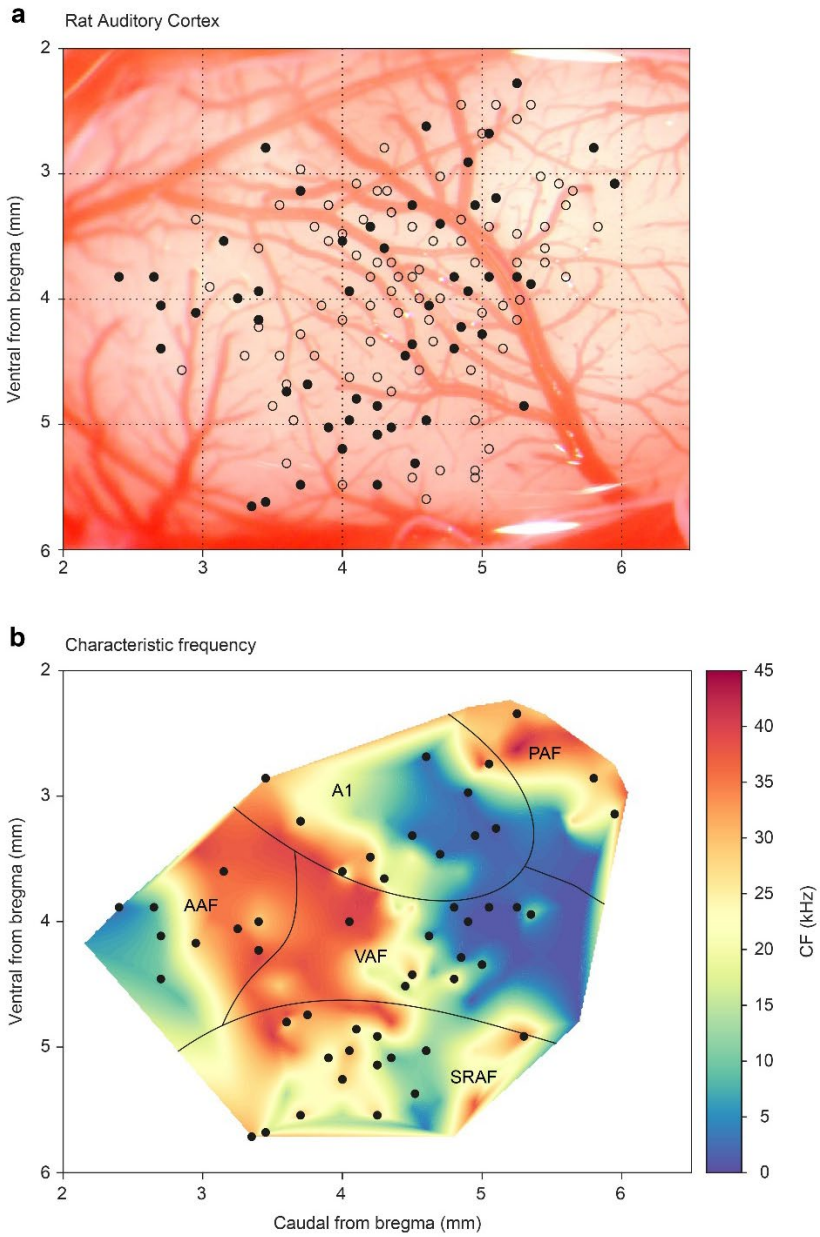


***Figure 1: Map of all recording locations***. *(a) All recording sites drawn over the cortex of a representative animal. At every site, the CF was determined and then we presented an oddball paradigm and the corresponding control sequences. (b) Distribution of the CFs across the*

142 *entire rat auditory cortex. Note how each field shows a characteristic CF*
143 *gradient. Empty dots indicate sites used only for CF determination. Filled*
144 *dots indicate sites where oddball paradigm was recorded.*

145

146 **ACh modulates the magnitude of neuronal responses and nMM**

147 After the FRA was identified, we selected a pair of pure tones (10–30 dB above minimum
148 threshold) within the FRA at each recording site to test the adaptation of the neuronal
149 response under the oddball paradigm. To do so we quantified nMM using the common SSA
150 index (CSI). CSI values may range from -1 to +1, with negative values for units that respond
151 more to standard stimuli and positive values for units that respond more to deviant stimuli
152 (see Methods). In the following, we describe the effect of ACh on nMM (Figs. 2-6), in terms
153 of prediction error modulation and repetition suppression (Fig. 7). Figure 2 illustrates
154 representative responses of two units from the lemniscal auditory pathway — during and after
155 the injection of ACh — that showed a change in the CSI during ACh release (Fig. 2a and b,
156 decreased and increased CSI, respectively). Similarly, the non-lemniscal, divisions (high-
157 order regions) of the AC (Fig. 3) also show decreased and increased CSI during ACh
158 application (Figure 3a and b; respectively). In both Figure 2 and 3, peri-stimulus time
159 histograms (PSTH) are also depicted for standard- and deviant stimuli (blue and red lines,
160 respectively). On average, the firing rate decreased during the application of ACh (mean
161 control: 5.8 ± 7.0 spikes/s, mean ACh: 4.7 ± 10.3 spikes/s; Wilcoxon Signed Rank test, $p <$
162 $0.001$). Most neurons recovered their basal firing rates after 60-90 minutes after the ACh
163 injection (recovery mean: 6.5 ± 8.1 spikes/s, Wilcoxon Signed Rank test, $p = 0.4$, control vs.
164 recovery).

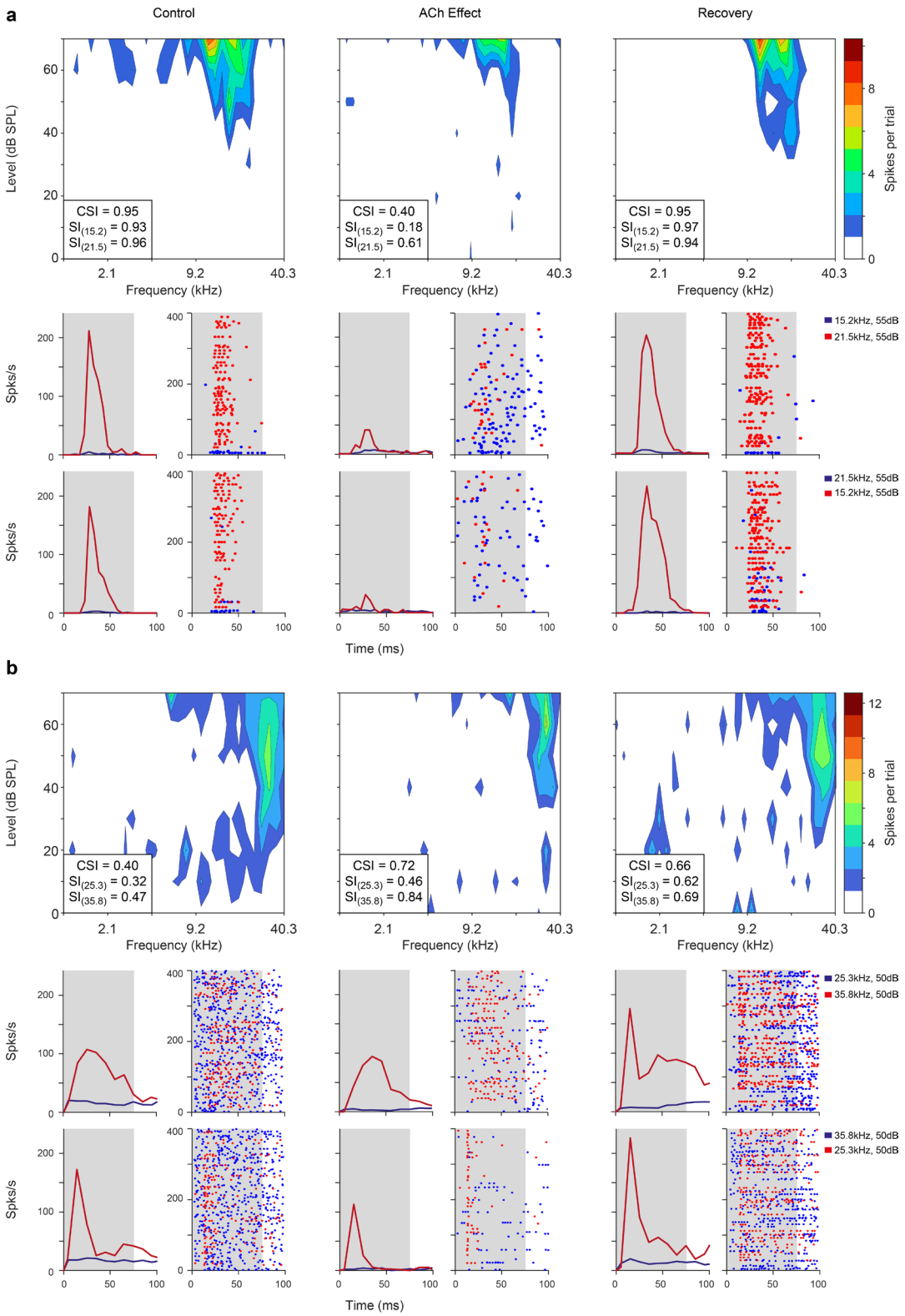


***Figure 2: Examples of lemniscal AC units modulated by ACh.*** *Left, middle and right columns show the responses before (control), during (effect) and after (recovery) ACh application, respectively.* ***a.*** *FRAs and*

*PSTHs from a unit located in A1. This specific neuron shows a CSI decrease during ACh application and recovery to baseline levels (CSI = 0.95, CSI= 0.4 and CSI = 0.95, respectively)* ***b.*** *FRAs and PSTHs from an AAF unit with increased CSI (CSI = 0.4, CSI= 0.72 and CSI = 0.66, respectively) during ACh application. Red lines and dots: deviant response; blue lines and dots: standard response.*

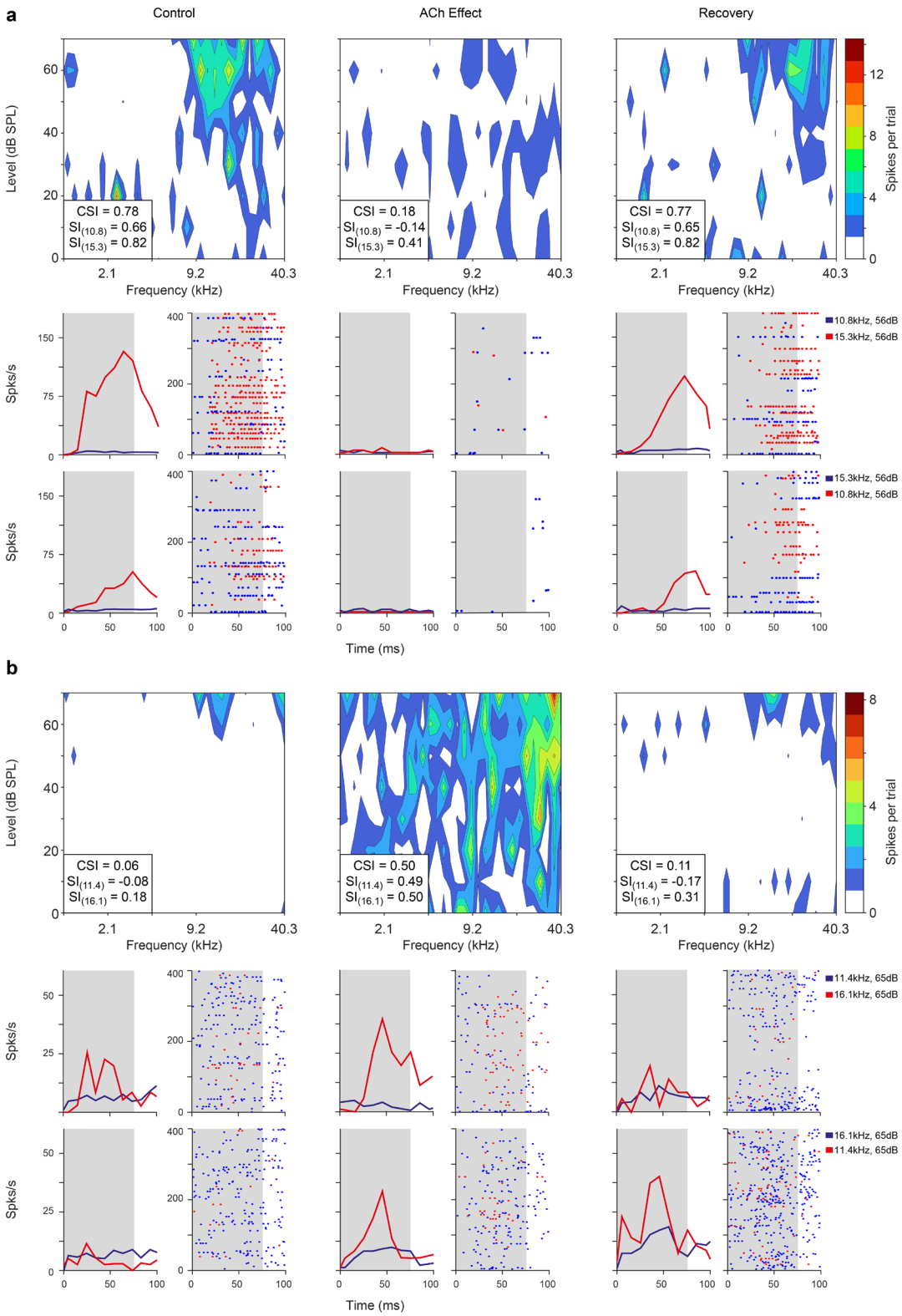


***Figure 3: Non-lemniscal AC units modulated by ACh.*** *Left, middle and right columns show the responses before (control), during (effect) and after (recovery) ACh application, respectively.* ***a.*** *FRAs and PSTHs from a unit*

*located in SRAF. This specific neuron shows a CSI decrease during ACh application and recovery to baseline levels (CSI = 0.78, CSI= 0.19 and CSI = 0.77, respectively).* ***b.*** *FRAs and PSTHs from a PAF unit with increased CSI (CSI = 0.06, CSI= 0.5 and CSI = 0.11, respectively) during ACh application. Red lines and dots: deviant response; blue lines and dots: standard response.*

Given the changes in the FRAs observed in individual units during the application of ACh (Figs. 2 and 3), we checked for bandwidth changes at the population level. For that, we measured the FRA bandwidth in octaves at 10 and 30 dB above minimum threshold (BW10 and BW30, respectively). Numerous individual units showed either broadening or sharpening of their FRA bandwidth during ACh application, which were averaged out at the population level (Fig. 4a,b). Indeed, no significant changes occur in neither BW10 (control: 0.76±0.57 octaves; effect: 0.88±0.75 octaves; Wilcoxon signed rank test, p = 0.248) nor BW30 (control: 1.33±0.73 octaves; effect: 1.43±0.80 octaves; Wilcoxon signed rank test, p = 0.664) (Fig. 4c).

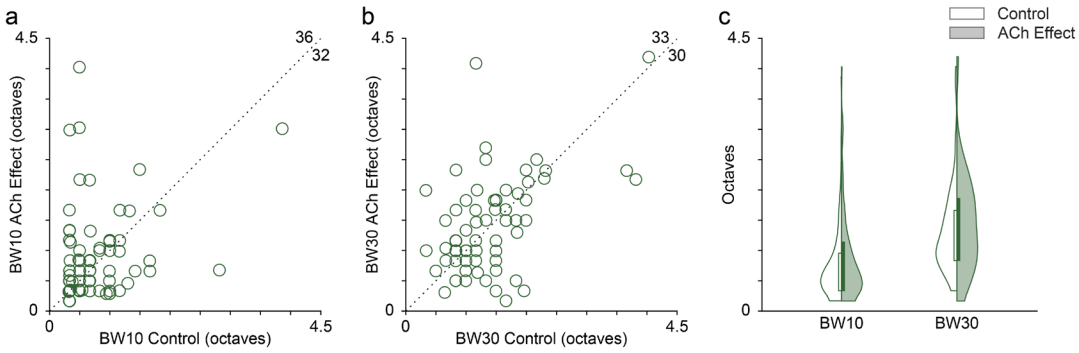


***Figure 4: Effect of ACh on the bandwidth of the FRAs.*** *Many individual units showed enlarged or reduced FRA bandwidths, both at 10 (a) and 30 (b) dB above minimum threshold. The values in the upper-right corner of panels (a) and (b) indicate the number of units showing either an increment*

*(top) or a decrement (right) of the bandwidth during the application of ACh. (c) Distribution of FRA bandwidths in octaves at 10 and 30 dB above minimum threshold (BW10 and BW30, respectively), before (white background) and during (shaded background) the application of ACh. ACh did not alter significantly neither BW10 nor BW30 at the population level.*

Next, we analyzed the effect of ACh on the CSI at the population level (n=85; comprising the neurons in our sample with significant responses to both F1 and F2 auditory stimuli). Figs. 2 and 3 illustrate four examples of units from lemniscal and non-lemniscal subdivisions before, during and after the application of ACh. Modulation of CSI levels was observed in all individual examples. ACh produced a significant increase of the CSI value in 26 % (Fig. 5a, purple dots; 22/85, bootstrapping, 95% *c.i.*) and a significant decrease in 31% of the neurons recorded (Fig. 5a, orange dots; 26/85, bootstrapping, 95% *c.i.*). Thirty-seven units (43%) were unaffected by ACh. The average CSI during ACh injection (CSI = 0.54 ± 0.27) was similar to that of the control condition (CSI = 0.57 ± 0.23; Wilcoxon Signed Rank test, p=0.359; Fig. 5b).

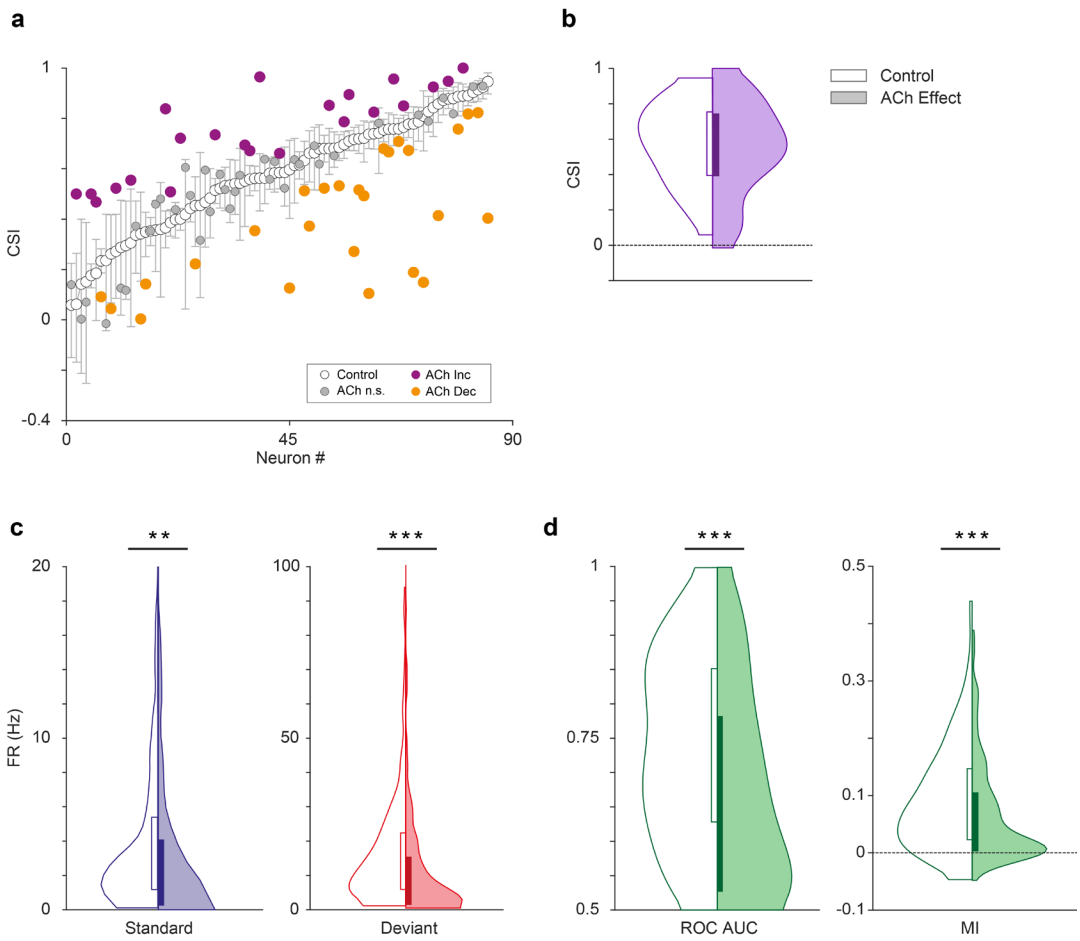


***Figure 5: Effect of acetylcholine on CSI***. *(a) Changes on the CSI due to the effect of ACh, for each recorded unit. The units are sorted based on their CSI in the control condition (white dots). The vertical bars indicate the 95% confidence interval for the CSI in the control condition. (b) Violin plots showing the CSI measured in control and effect conditions. The CSI did not change significantly during the application of ACH. In this and similar violin plots, white background indicates the control conditions, while shaded background indicates the effect condition. (c) Distribution of firing rates in response to the deviant (red) and standard tones (blue), in control and ACh conditions. The application of ACh caused a significant reduction in the response to both deviant and standard tones. (d) Distribution of AUC and Mutual Information values in control and ACh conditions. The application of ACh caused a significant*

*decrease of both AC and Mutual Information. In this and similar figures: *p<0.05; **p<0.01; ***p<0.001.*

We analyzed the effect of ACh on the response to the deviant- or standard stimuli, separately. We observed that ACh produced a significant decrease in the mean firing rate in response to the deviant tones (Fig. 5c; 11.75 ±17.46 Hz), as compared to the control condition (16.51 ±16.19 Hz; Wilcoxon Signed Rank test, $p < 0.001$), as well as in the mean firing rate in response to standard tones (Fig. 5c; 4.58 ±6.38 vs 3.97 ±9.90 Hz, control vs ACh; Wilcoxon Signed Rank test, $p = 0.001$).

In order to establish how ACh affects discriminability of deviant- and standard stimuli — i.e. how well the stimulus identity can be decoded from the neuronal firing rate – we calculated the area under the curve (AUC) of the receiver operating characteristic (ROC) for each tone (Fig. 5d, left panel) and the Mutual Information to determine how much the response distributions for deviant- and standard stimuli overlap before and after ACh injections and how well the stimulus identity can be decoded from the neuronal firing rate. AUC indicates how different the neuronal responses to deviant- and standard stimuli are, and thus, how well a neuron is able to discriminate between both types of stimuli, considering that the neuron would respond differently to them (in terms of firing rate). Completely overlapping firing rate distributions (in response to deviants and standards) would yield an AUC = 0.5, while separate distributions would result in AUC = 1. On the other hand, Mutual Information is defined as the reduction in the uncertainty of one variable (in this case the neuronal response) due to the knowledge of another (in this case, the type of stimulus; Timme and Lapish, 2018). In other words, this measure reflects how much information a neural response (firing rate) contains about the type of stimulus that is played. In practical terms, high Mutual Information

implies that a neuron is able to discriminate between stimuli, and thus respond differently to them. This analysis shows that the mean AUC decreased significantly during the application of ACh (0.74 ±0.13 vs 0.67 ±0.15, control vs. effect; Wilcoxon Signed Rank test, $p < 0.001$). The same happened for Mutual Information (Fig. 5d, right panel; 0.09 ±0.07 vs 0.07 ±0.08, control vs. effect; Wilcoxon Signed Rank test, $p = 0.003$). These AUC and Mutual Information analyses indicate that under the influence of ACh, neurons are less able to discriminate deviant stimuli from standard stimuli.

**Different mechanisms for SI increase or decrease during ACh application**

As mentioned above, the CSI is an indicator of the average level of nMM for a single unit, since it takes into account the responses of two frequencies (F1 and F2) that alternatively play the role of deviant and standard. However, in order to better understand the effect of ACh on the response to each stimulus class — depending on whether it was presented as a deviant or as a standard — the frequency-specific SSA index (SI, see Methods) is a better indicator. We calculated the SI for 205 individual frequencies, from 113 units that elicited a significant response to that particular frequency from our sample. This analysis shows that ACh produced a significant increase of the SI in 27% of the frequencies recorded (Fig. 6a, purple dots; 55/205, bootstrapping, 95% *c.i.*), 31% (64/205; Fig. 6a, orange dots) showed a significant decrease of their SI and 42% frequencies (86/205) were unaffected by ACh. The mean SI (SI = 0.55 ± 0.31, control condition) was reduced during ACh injection (SI = 0.40 ± 0.50) although this decrease was not significant (Wilcoxon Signed Rank test, $p=0.086$; Fig. 6b).

Since we found that the application of ACh had divergent effects on the SI (increase or decrease), we further analyzed separately those two groups to identify different mechanisms.

280 We examined the firing rates in response to deviant- and standard stimuli, separately for those
281 frequencies showing a SI increase or decrease during the application of ACh. In both cases,
282 responses to the deviant- and standard stimuli were affected differently, when measuring the
283 firing rate change ratio (amount of change caused by ACh, relative to the baseline firing rate).
284 In frequencies showing SI decrease, the effect of ACh was significantly different for the
285 deviant- and standard stimuli (Fig. 6c, top panel; $p<0.001$, Wilcoxon signed rank test).
286 Furthermore, this ratio was clearly negative for deviant sounds ($p<0.001$, Wilcoxon signed
287 rank test) and not significant for standards ($p=0.256$, Wilcoxon signed rank test), indicating
288 that ACh caused a reduction of the firing rate differentially during deviant stimuli. On the
289 other hand, in frequencies showing SI increase the effect of ACh also had a distinct effect on
290 the deviant- and standard stimuli (Fig. 6d, top panel; $p<0.001$, Wilcoxon signed rank test), but
291 in this case the effects were reverse: the change ratio was clearly negative for standard sounds
292 ($p=0.001$, Wilcoxon signed rank test) and not significant for deviant ones ($p=0.379$, Wilcoxon
293 signed rank test), hence ACh caused a reduction of the firing rate primarily during standard
294 stimuli. In other words, while the effect of ACh was a reduction of the firing rate, in some
295 frequencies it only affected responses to the deviant stimuli, thus decreasing SI (Fig 6c, top
296 panel), while in others it only affected responses to the standard stimuli, resulting in an
297 increment of the SI (Fig 6d, top panel).

298 Interestingly, stimuli discriminability was affected differently by ACh in both groups. In
299 frequencies showing SI decrease (Fig. 6c, bottom panel) both ROC AUC and Mutual
300 Information decreased significantly during ACh application ($p<0.001$in both cases, Wilcoxon
301 signed rank test), in line with the results obtained for the whole sample (compare to Fig. 5d).
302 However, in frequencies showing SI increase (Fig. 6d, bottom panel) ROC AUC did not
303 change significantly ($p= 0.339$), while Mutual Information increased slightly ($p= 0.008$).

304 These results suggest that frequencies showing SI decrease are the ones mediating the main

305 effects of ACh in the population.

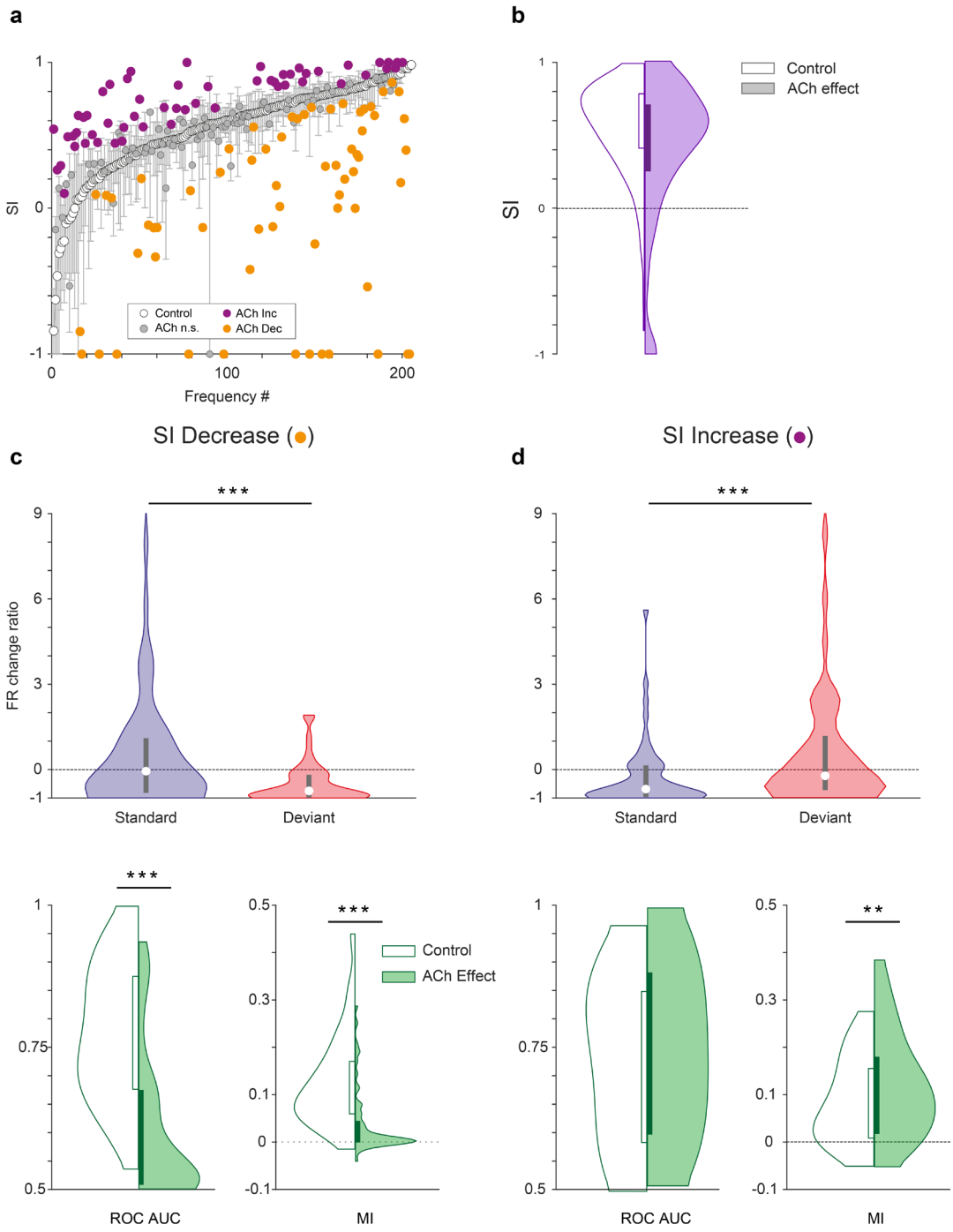


306

307 ***Figure 6: Characteristics of units depending on the effect of ACh on SI.*** *(a)*

308 *Changes on the SI due to the effect of ACh, for each tested tone. The units are sorted*

309 *based on their SI in the control condition (white dots). The vertical bars indicate the*

*95% confidence interval for the SI in the control condition. (b) Violin plot depicting the overall effect of ACh on the SI, for the complete sample. (c) Firing rate change ratio due to ACh application, relative to the control condition. In units showing SI decrease (left column), it was caused by a significant reduction of the firing rate in response to deviant tones. By contrast, in units showing SI increase (right column) it was caused by a significant reduction of the firing rate in response to standard tones. (d) In units showing SI decrease (left column) there was a significant reduction of both AUC and Mutual Information during the application of ACh. On the other hand, in units showing SI increase (right column) AUC did not change but Mutual Information increased.*

**ACh affects neuronal mismatch, modulating prediction error responses but not repetition suppression**

According to the predictive coding framework, nMM can be split in two functionally distinct components: prediction error modulation (i.e., an increased response to an oddball caused by the violation of a regularity) and repetition suppression (i.e., reduction in the response to a standard caused by sensory learning of a repeated stimulus). These differential effects can be quantified by comparing the responses to the oddball paradigm with a suitable control sequence (Fig. S1). Therefore, to test if ACh modulates prediction error signaling in AC, we also recorded the cascade control sequence (for the corresponding oddball sequences) in 66 neurons of the sample, using an approach previously published (Carbajal and Malmierca, 2018; Parras et al., 2017; Ruhnau et al., 2012; Valdés-Baizabal et al., 2019). First, we calculated the normalized spike counts in response to the cascade control, deviant and standard stimuli (CAS, DEV and STD, respectively; see Methods). ACh led to a significant

decrease in the DEV responses in those units where SI decreased (Fig 7a; Wilcoxon Signed Rank test, p<0.001) and to a significant increase in those units were SI increased (Fig 7b; p= 0.011). The opposite effect occurs on STD stimuli, increasing in units where SI decreased (Fig 7a; p<0.001) and decreasing in units where SI increased (Fig 7b; p<0.001). While this trend is very clear, there were no significant changes in CAS (p=0.091 and p = 0.072, for SI decrease and increase, respectively).

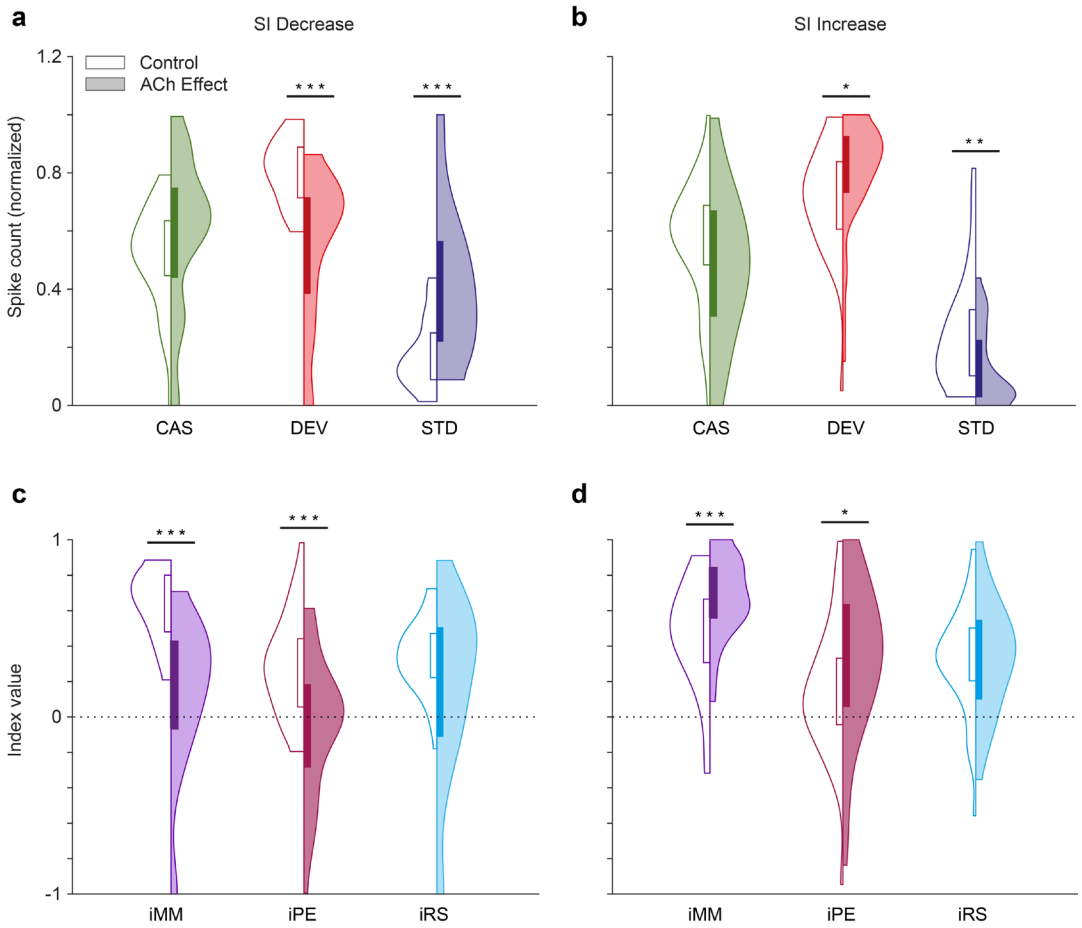


***Figure 7: Predictive coding indices depending on the effect of ACh on SI.*** *The application of ACh decreased the normalized spike counts in response to deviant stimuli (red) and increased the normalized spike counts in response to standard stimuli (blue) in those units where SI decreased due to*

*the application of ACh (a), while the changes were opposite in those units where SI increased due to the application of ACh (b). In neither case, did the response to the cascade condition (green) change significantly, but there was a slight trend in the same direction as the changes of the standards. In consequence, the neuronal mismatch (iMM, purple) and prediction error indexes (iPE, light red) decreased significantly in those units where SI decreased due to the application of ACh (c), but increased in those units where SI increased due to the application of ACh (d). The repetition suppression index (iRS) in light blue, did not change significantly in any case.*

Using the normalized CAS, DEV and STD responses, we computed the indexes iMM, iPE and iRS before and after the ACh injection in SI decrease units (Figure 7c, iMM: 0.63 ± 0.19 vs 0.13 ± 42; iPE: 0.29 ± 0.27 vs -0.05 ± 0.38; iRS: 0.34 ± 0.20 vs 0.17 ± 0.49; control vs ACh, respectively) and SI increase units (Figure 7d, iMM: 0.47 ± 0.31 vs 0.67 ± 0.22; iPE: 0.15 ± 0.36 vs 0.33 ± 43; iRS: 0.32 ± 0.30 vs 0.34 ± 0.31). iMM is equivalent to the CSI, but using normalized response values, and since it includes information about the cascade control, it can be divided into prediction error and repetition suppression components (iPE and iRS, respectively; see Methods and Fig. S1c). Significant effects of ACh administration were found for iMM and iPE, both in SI decrease units (iPE: $p<0.001$; iMM: $p<0.001$; Wilcoxon Signed Rank test; Fig. 7c) and SI increase units (iPE: $p = 0.023$; iMM: $p<0.001$; Wilcoxon Signed Rank test; Fig. 7d), while iRS remained unchanged (SI decrease units iRS: $p = 0.121$; SI increase units iRS: $p = 0.675$; Wilcoxon Signed Rank test).

369 Under the predictive coding framework, the precision of prediction errors encodes the
370 confidence or reliability afforded such errors (Friston, 2008), enabling precise prediction
371 errors to access higher levels of the auditory hierarchy. To test whether neuronal responses
372 show differential effects of precision weighting — depending on their level of deviance
373 sensitivity – we split our sample in two similar-sized groups (of frequencies), using the
374 median SI as cutoff (0.6143: SI before the application of ACh): low SI (n = 65 frequencies
375 with cascade control) and high SI (n = 66 frequencies with cascade control) (Fig. 8a-c). Given
376 this grouping, we found that ACh decreased significantly iMM (0.72±0.13 vs 0.52±0.36,
377 control vs effect; $p<0.001$) and iPE (0.33±0.33 vs 0.145±0.48, control vs effect; $p=0.004$) in
378 high SI frequencies, while only decreasing iRS significantly in low SI frequencies (0.28±0.25
379 vs 0.18±0.36, control vs effect; $p<0.037$) (Fig. 8a-c, top row).

380 Given the divergent defects of ACh on putative prediction error modulation we hypothesized
381 that acetylcholine would increase the variance of deviance-sensitive responses over groups of
382 cells. We calculated the variance of the above distributions of predictive coding indexes
383 (iMM, iPE and iRS) as an estimate of the (inverse of) their precision, as well as its 95%
384 confidence interval using a 1000-sample bootstrap strategy, and then used an F-test to check
385 for differences in the variances before and during ACh application (Fig. 8a-c, bottom row).
386 These results demonstrate that ACh application significantly increases the variance of iMM
387 and iRS for both low SI and high SI groups, but interestingly ACh also significantly increase
388 the variance of iPE only for the high SI group.

389 Then, we repeated the same variance analysis grouping the frequencies based on the
390 anatomical layer location (depth) of the recording sites (Fig. 8d-f). In this case we split the
391 frequencies into deep and superficial, with a depth cutoff of 650 μm, which is near the
392 boundary between layers IV and V in the rat AC (Games and Winer, 1988; Malmierca, 2015).
393 In this case, we found no significant effect of ACh on iMM, iPE nor iRS for none of the depth

394 groups (Fig. 8d-f, top row). However, the general trend was an increase in the variance for all
395 indexes and depth groups during the application of ACh (except for iPE in superficial units),
396 which was significant for all indexes in the case deep units only (Fig. 8d-f, top row).

397 Thus, our results indicate that ACh produces a general increase of the variance for iMM, iPE
398 and iRS. This general increase occurs regardless of the baseline SI value, but is more
399 noticeable for neurons located in the infragranular layers.

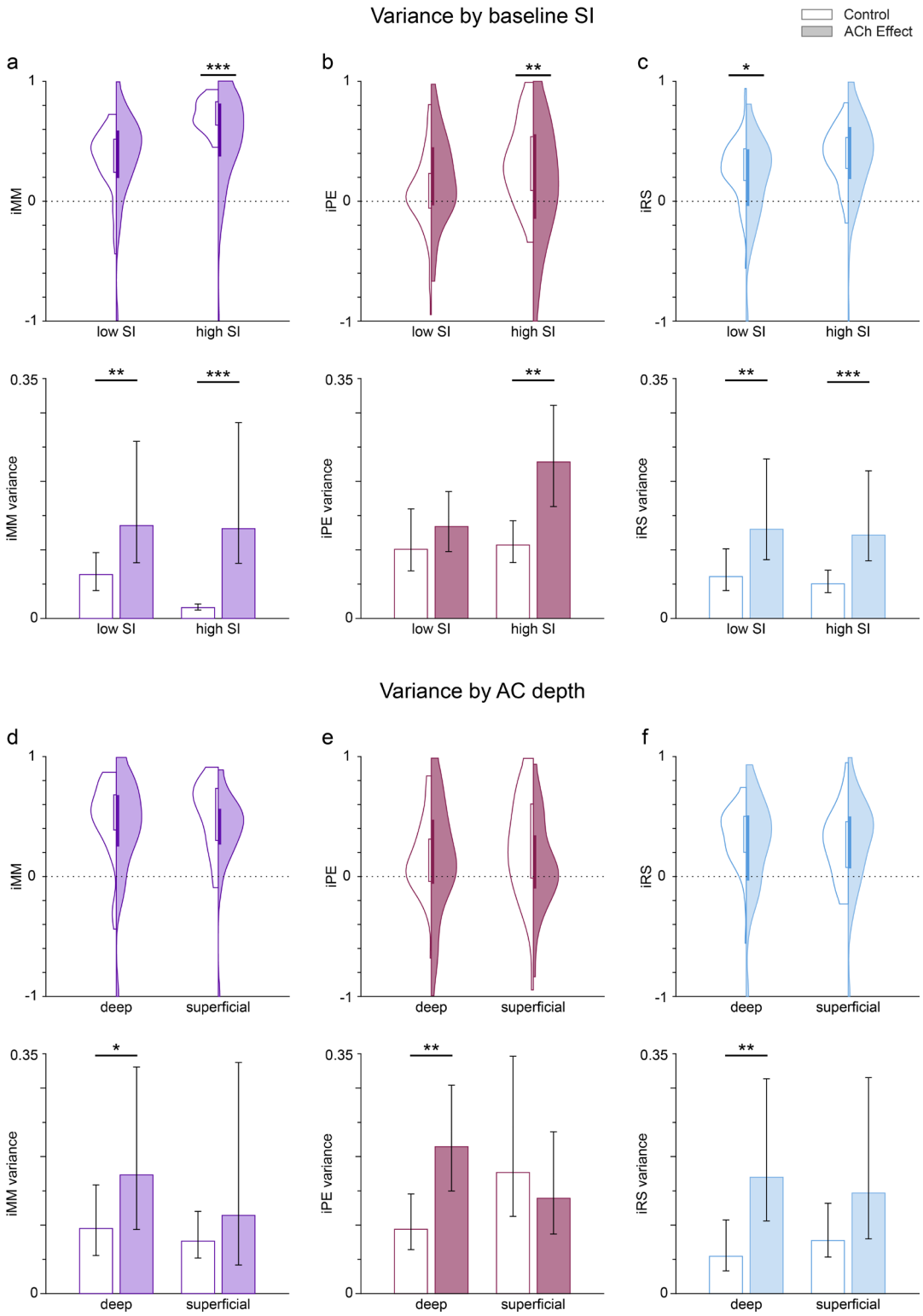


400

401 ***Figure 8: Dependence of the variance of predictive coding indexes on the SI before ACh***

402 ***application, as well as and on AC depth***. *Violin plots show the distribution of the iMM, iPE*

403 *and iRS indexes based on the SI value before application (a-c; low SI: SI < 0.6143; high SI:*

404 *SI < 0.6143, see text) or the AC depth (d-f; deep: >650 µm; superficial: <650 µm). Bar*

*graphs show the variance of the related indexes. Error bars indicate 95% CI. The results before ACh application are shown in a white background (control), while shaded backgrounds represent the results during ACh application (effect). The application of ACh reduced significantly iMM and iPE (a and b, top row) for those frequencies with high baseline SI, as well as iRS (c, top row) for frequencies with low baseline SI. The variance of all indexes increased significantly during ACh application, except for the iPE of the low SI group. Regarding the depth of the recording sites, ACh did not significantly change the values of any indexes, neither for deep nor for superficial units (d-f, top row). However, ACh significantly increased the variance of all indexes for deep units, but not for superficial units (d-f, bottom row).*

**ACh effect on nMM as a function of topographic distribution**

A remaining question is whether the effect of ACh is uniformly distributed across AC neurons in different fields and layers. Figure 9 shows the CSI (first row) and spike count levels for the standard and deviant tones (middle and bottom rows, respectively) before and after ACh application, as well as the difference between the ACh and control conditions. The highest levels of CSI in the control condition (left column) were found in SRAF. ACh application (middle column) produced an overall increment of CSI in AAF and a decrement in the rest of the fields, however such changes did not reach statistical significance ($p>0.79$ in all fields, Wilcoxon signed rank test with Holm-Bonferroni correction). Regarding the responses to the standard stimuli (middle row), ACh application caused an increase of the firing rate in A1 and PAF, and a decrease in AAF, VAF and SRAF, but such changes were only significant in AAF ($p=0.001$, Wilcoxon signed rank test with Holm-Bonferroni correction). By contrast, the firing rates in response to the deviant sounds (bottom row) decreased in all fields during ACh

application, with significant changes in AAF, VAF and SRAF (p=0.011, p=0.026 and p=0.009, respectively; Wilcoxon signed rank test with Holm-Bonferroni correction).

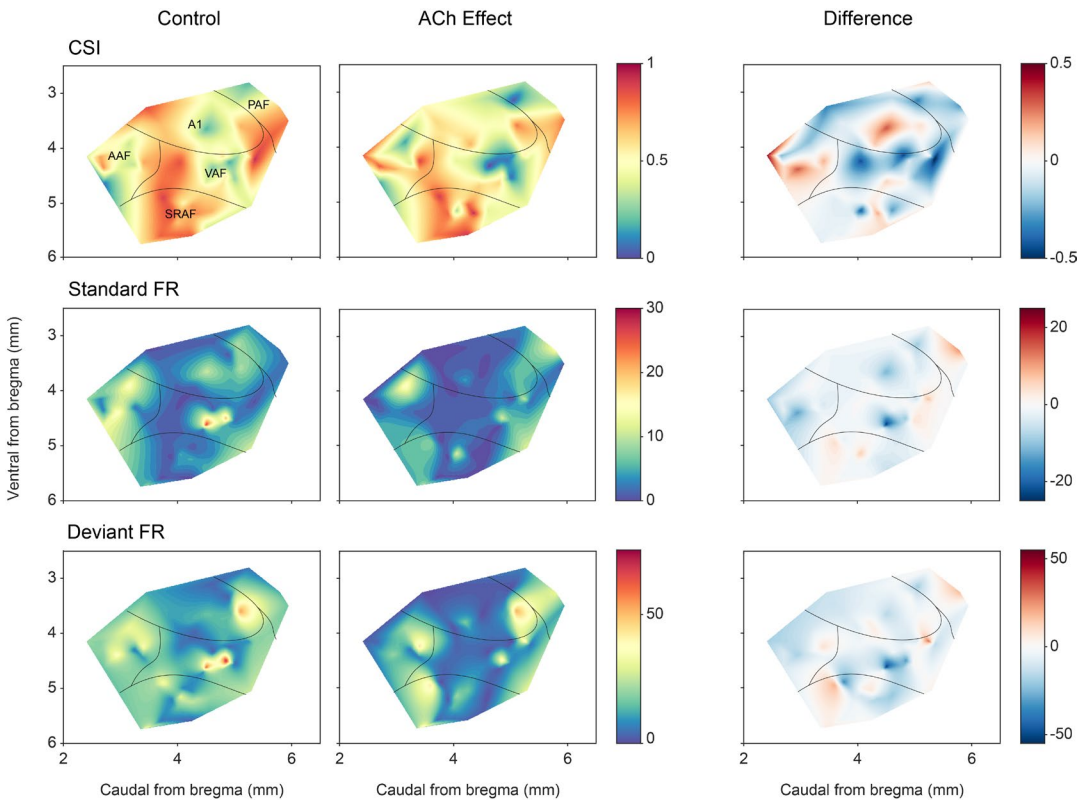


***Figure 9: Anatomical localization of CSI and responses to the deviant and standard tones****. Distribution of CSI (top row) and responses (spikes per trial) for deviant (bottom row) and standard tones (middle row), before and after ACh application, as well as the difference between both conditions.*

In order to better understand the effect of ACh on the responses to the individual frequencies of the oddball paradigm (F1 and F2), we calculated the SSA index (SI) independently for each of the paradigm frequencies. We found that ACh was more likely to cause a SI decrease in all AC fields except for AAF, where ACh was more likely to cause an SI increase (Fig. 10a). Figure 10b shows the distribution of recording depths within the AC, for those units that showed a significant SI decrease (orange) or increase (purple) during the application of ACh.

The shaded background shows the probability density function for those distributions. We found that frequencies that experienced an SI decrease during ACh application were most likely located in the granular layer (layer IV) or the upper infragranular regions (dorsal parts of layer V). In contrast, frequencies that experienced an SI decrease during ACh application were more likely located in deeper infragranular regions (layers V and VI).

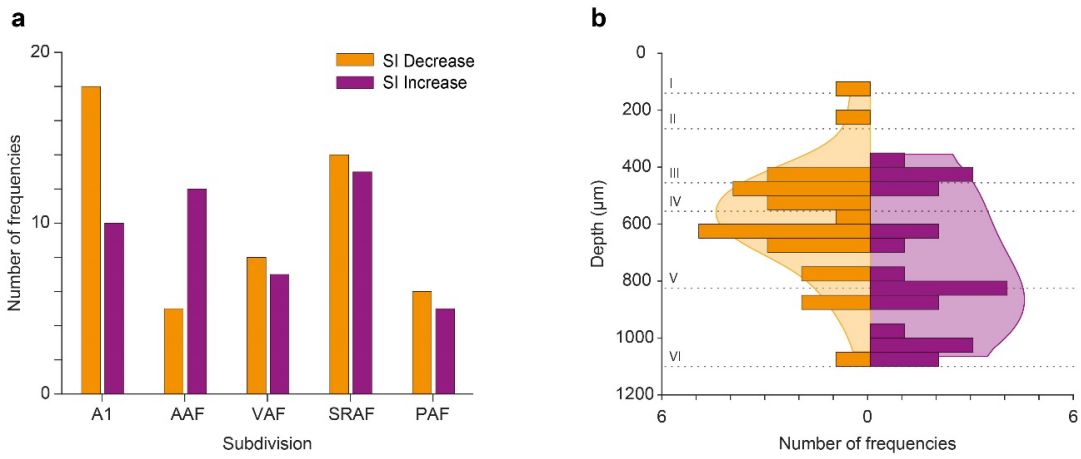


***Figure 10: Effect of ACh on* nMM *in AC fields and layers.*** *(a) Number of tested frequencies in which SI decreased (orange) or increased (purple) for each AC field. In A1 it is more likely to find frequencies showing SI decrease, while in AAF it is more likely to find those showing SI increase. In VAR, SRAF and PAF, the likelihood of both types is similar. (b) Distribution of tested frequencies in which SI decreased (orange) or increased (purple) significantly due to the effect of ACh, across AC layers. The shaded background depicts the probability density functions. Note that units experiencing SI decrease are more prevalent around the granular layer (layer IV), while units experiencing SI increase are more commonly found in the infragranular layers.*

## DISCUSSION

We recorded neuronal responses from the AC under an auditory oddball paradigm while performing microiontophoretic applications of ACh to investigate the role of the cholinergic system in the processing of unexpected or surprising events. Furthermore, we employed cascade sequences to control for repetition suppression and assess cholinergic effects on prediction error relative to repetition suppression. Our results show that 1) ACh modulates nMM, evidenced as decrements or increments of the neuronal mismatch indexes (iMM, iPE and iRS). The decreased SI is due to a diminished response to the deviant tone while increased SI is the consequence of a diminished response to the standard sounds (Fig. 6, and examples in Figs. 2-3); 2) ACh exerts a global and distributed effect on AC neurons that is layer specific but field unspecific (Figs. 9,10); 3) The decreased- and increased SI are driven by the effects of ACh on iPE but not iRS (Fig. 7), and 4) ACh increases the variance of iMM, iPE and iRS. Together, these findings reveal how ACh modulates prediction error signals and repetition suppression differentially in the AC, likely gating these signals, as they ascend beyond the auditory cortex to frontal, higher cognitive regions.

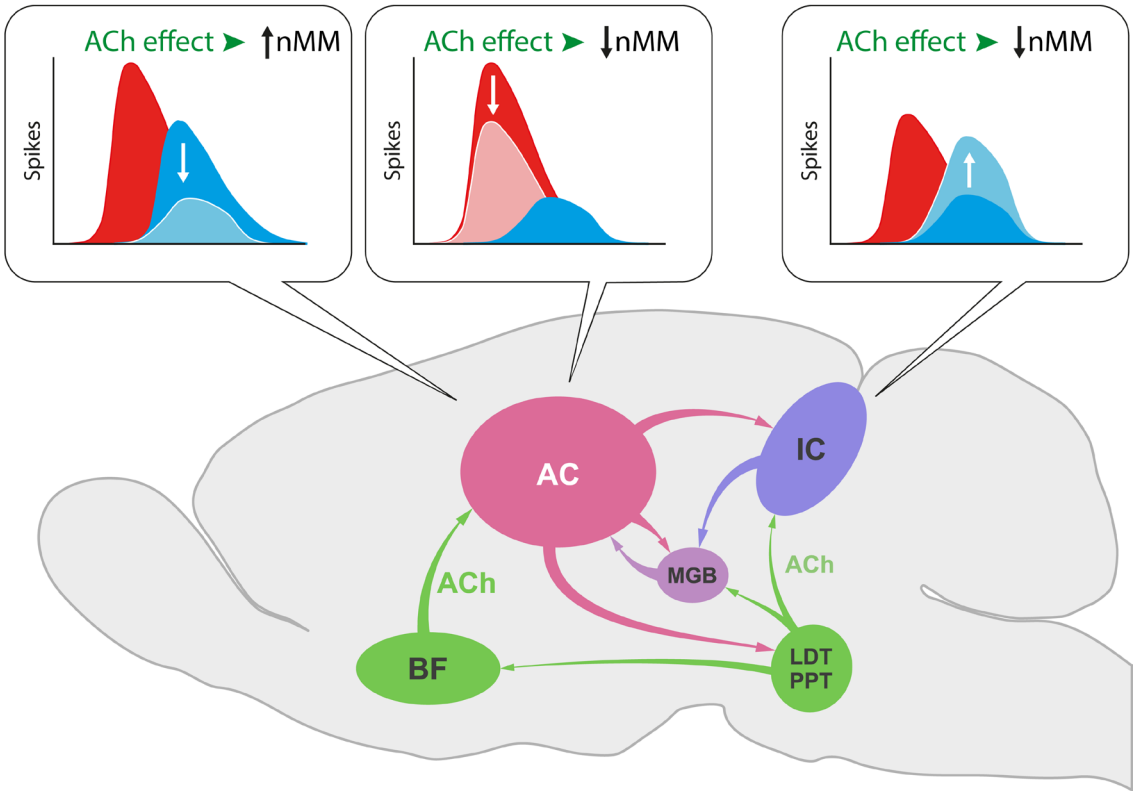


***Figure 11: Effect of ACh on nMM in auditory midbrain and cortex.*** *ACh increases nMM in the AC reducing the firing rate in response to either 'deviants' or 'standards', while it shows a different effect in the IC, as ACh decreases nMM by increasing the responses to the 'standard' tones (Ayala and Malmierca, 2015). These divergent effects may be explained by the different connectivity of both auditory areas. While the AC receives its cholinergic input from the basal forebrain (BF), the IC is innervated by the pedunculopontine (PPT) and laterodorsal tegmental (LDT) regions in the brainstem. This intersection of auditory and cholinergic nuclei creates an intricate network involving ascending and descending projections that ultimately modulate the processing of auditory deviance detection.*

ACh increases the amplitude of AC neuronal responses to sound stimulation, decreases the auditory threshold and sharpen the receptive field in the AC. (Edeline, 2012; Irvine, 2018a,

494 2018b; Kilgard and Merzenich, 1998; Ma and Suga, 2005; Metherate, 2011; Metherate et al.,
495 1992; Puckett et al., 2007). These ACh-mediated effects are produced by a rapid disinhibition
496 of neuronal responses, modifying synaptic strength, enhancing excitatory-inhibitory balance
497 and reorganizing cortical circuits promoting cortical plasticity (Froemke et al., 2007; Irvine,
498 2018a, 2018b; Metherate, 2011; Picciotto et al., 2012). But ACh also produces direct
499 inhibitory effects leading to a decrease of cortical responses (Colangelo et al., 2019; Dasgupta
500 et al., 2018; Eggermann and Feldmeyer, 2009; Qi and Feldmeyer, 2022). Our results confirm
501 these mixed effects (excitatory and inhibitory, during the application of ACh) at the neuronal
502 level. However, when looking at the population level, the overall effect in our sample was a
503 differential reduction of the responses to either deviant or standard stimuli. Apart from the
504 direct hyperpolarizing effect of ACh on some cell types, it is also possible that some of the
505 recorded neurons received direct inhibitory inputs, and those inhibitory neurons were the ones
506 affected by ACh. By increasing the firing rates of such inhibitory interneurons, the observed
507 overall effect of ACh could lead to a reduction of the activity on the recorded neurons. An
508 important functional motif — for state modulation in the cortex — is through disinhibition
509 consisting of parvalbumin-, somatostatin-, and vasoactive intestinal peptide- expressing
510 interneurons. When the latter receive cholinergic projections from the basal forebrain, they
511 remove the inhibition on layer 2/3 pyramidal neurons exerted by somatostatin interneurons (Fu et
512 al., 2014). The connectivity relationships among inhibitory neurons seems to be critical.
513 Moreover, it has been recently described how each of those cell types respond differently to
514 deviants and standards in the auditory cortex (Yarden et al., 2022). ACh plays important roles
515 in arousal, attention, and sensory learning (Hasselmo, 1999; Hasselmo and Sarter, 2011;
516 Metherate, 2011; Picciotto et al., 2012; Sarter et al., 2001; Weinberger, 2004). Thus, it is not
517 surprising that ACh may have a critical role in shaping nMM, which has many properties in
518 common with behavioral habituation to a repeated stimulus and can be considered a simple
519 form of learning (Irvine, 2018a; Nelken, 2014; Netser et al., 2011). Furthermore, a recent

study in rats has shown that the administration of muscarinic ACh receptor agonists and antagonists affected MMN amplitude in A1 and PAF (Schöbi et al., 2021), suggesting that the cholinergic system modulates the connectivity between those areas during the occurrence of deviant sounds. But to the best of our knowledge, the present study demonstrates a specific effect of ACh on prediction error responses.

In the IC, ACh selectively increased the response to the repetitious standard stimulus (Ayala and Malmierca, 2015), while we show here that ACh in the AC not only increases the responses to the unexpected deviant sounds leading to an increase of SI (Fig. 6d) but also decreases responses to the repeated standard that result in a diminished CSI index (Fig. 6c). This divergent effect of ACh on subcortical and cortical nMM may be related to the different origin of ACh and/or the unique organization of neuronal circuitries in IC and AC (Fig. 11). While the sources of ACh to IC emerge from the pedunculopontine and laterodorsal tegmental regions in the brainstem (Motts and Schofield, 2009), those to AC originate in the basal forebrain (Chavez and Zaborszky, 2017).

According to the predictive coding formulations, cortical areas send predictions to lower hierarchical areas to inhibit neuronal populations encoding prediction errors. When top-down predictions match bottom-up sensory input, the prediction error response is attenuated. Conversely, those lower areas send error information to higher hierarchical centers when event predictions fail to drive higher level representations and improve the top-down predictions. If a stimulus is not predicted, the difference between predicted and received inputs yields large prediction errors, while if a stimulus is constantly repeated, sensory learning enables more accurate predictions and a decrease in prediction error responses – a phenomenon referred to as repetition suppression (Auksztulewicz and Friston, 2016). Thus, nMM can be explained under the predictive coding framework (Carbajal and Malmierca, 2018; Parras et al., 2017), and recent studies that found LFP and spiking responses to omitted

545 tones in the rat auditory cortex (Auksztulewicz et al., 2023; Lao-Rodríguez et al., 2023),
546 among others, strongly support this interpretation. However, predictions and prediction errors
547 may also be modulated in a context-dependent manner, meaning that responses can be
548 modulated and given precedence depending on the context in which the stimulus is perceived
549 (Keller and Mrsic-Flogel, 2018). The source of such a modulating or gating signal may arise
550 from neuromodulatory inputs (Fu et al., 2014; Moran et al., 2013; Pinto et al., 2013; Polack et
551 al., 2013; Thiele and Bellgrove, 2018) that can not only gate plasticity (Kilgard and
552 Merzenich, 1998; Martins and Froemke, 2015; Weinberger, 2004), but also change the
553 balance of top-down versus bottom-up influence (Yu and Dayan, 2002).

554 Within the predictive coding framework, classical neuromodulators such as ACh are often
555 thought to increase the precision of prediction error signaling (Auksztulewicz et al., 2018;
556 Auksztulewicz and Friston, 2016; Feldman and Friston, 2010; Moran et al., 2013). Indeed, Yu
557 and Dayan (Yu and Dayan, 2005, 2002) proposed that ACh levels reflect the "expected
558 uncertainty" (when there is less confidence in the prediction) associated with top-down
559 information and modulate the interaction between top-down and bottom-up processing in
560 determining the appropriate neural representations for inputs (Auksztulewicz et al., 2017; Yu
561 and Dayan, 2005, 2002). Thus, the precision of prediction errors would encode the confidence
562 or reliability afforded of such errors (Friston, 2005), increasing the influence of precise
563 prediction errors on higher-level processing. Thus, the canonical view – within the predictive
564 coding framework — is that precision would affect postsynaptic gain through the action of
565 neuromodulators such as ACh, enhancing the responses of units broadcasting prediction
566 errors. Using computational neuronal modeling and EEG recordings under oddball paradigms
567 in subjects manipulated pharmacologically with galantamine (a competitive inhibitor of
568 acetylcholinesterase, Moran et al. (2013) have shown that ACh enhances the precision of
569 bottom-up synaptic transmission in cortical hierarchies by optimizing the gain of

supragranular pyramidal neurons, amounting to an increase in the precision of prediction error signaling. Thus, our results and those from Moran and colleagues (2013) suggest that ACh mediates the representation of precision.

Our results are consistent with this predictive coding picture; particularly when noting that and increase in precision leads to a representational sharpening (Kok et al., 2012a), in which the majority of (prediction error) neurons are suppressed and a few neurons encoding precise prediction errors are enhanced (Friston, 2018; Kok et al., 2012a; Shipp, 2016). This is consistent with the effect of acetylcholine on average over neurons studied and the differential effect on standard and oddball responses; dependent upon their SI.

ACh increases the variance the prediction error component of neuronal responses in those units with higher SI (Fig. 8b, top), especially in units with strong deviance detection properties (Fig. 8b, bottom). This finding suggests that ACh plays the key role in encoding of precision or uncertainty. Interestingly, ACh not only increases the variance of prediction error responses, but also the variance of repetition suppression (Fig. 8c).

A change in the precision of prediction errors may denote — or alert to — a variable environment, where it is difficult to extract rules and only generate weak (and less useful) predictions. Under this scenario, some fluctuations in the sensory input can be expected, assigning less precision to prediction errors (Yon and Frith, 2021). If so, ACh would adjust the predictions' confidence, so we would not be surprised by small changes in the environment, since they are likely, expected noisy, fluctuations. Otherwise, an excessive confidence on predictions in a volatile environment may override the incoming evidence, leading to the false inference of expected by absent events (Yon and Frith, 2021). Attention is thought to boost the precision of prediction errors (Kok et al., 2012b), and our experiments carried out under anesthesia clearly lack attention, where baseline cholinergic activity is low,

making it difficult to interpret how the results generalize to more ecologically valid situations (Minces et al., 2017). Interestingly, there is a wealth of data suggesting that minimal impairments to the encoding or defective signaling of precision or uncertainty are sufficient to explain psychopathic conditions such as schizophrenia or autism (Friston, 2023). Furthermore, while we are not aware of any known direct connection between auditory processing disorders and ACh, individuals with auditory processing disorders do have difficulties with auditory selective attention, so perhaps one could speculate that ACh, by modulating SSA/prediction error, could impact encoding of salient events, and if disrupted could lead to problems with selective attention. Moore (2012) speculated that auditory processing disorders may arise from unbalanced processing in bottom-up and top-down contributions, i.e., there might be some aspects of predictive processing altered. A recent study (Felix et al., 2019) analyzed altered temporal processing at the level of the brainstem in $\alpha_7$-subunit of the nicotinic acetylcholine receptor ($\alpha_7$-nAChR)-deficient mice. After studying $\alpha_7$-nAChR knockout mice of both sexes and wild-type colony controls, they concluded that the malfunction of the *CHRNA7* gene that encodes the $\alpha_7$-nAChR may contribute to degraded spike timing in the midbrain, which may underlie the observed timing delay in the ABR signals. These authors (Felix et al., 2019) proposed that their findings are consistent with a role for the $\alpha_7$-nAChR in types of neurodevelopmental and auditory processing disorders. There is also evidence of cholinergic system disfunction being related to the pathophysiology of Alzheimer's disease (Pérez-González et al., 2022). For instance, disfunction of the synapses of cholinergic neurons in the hippocampus and nucleus basalis of Meynert, as well as decreased choline acetyltransferase activity, is associated to memory disorders in Alzheimer's disease (Hampel et al., 2018). Also, Alzheimer's disease patients show reduced amounts of the vesicular ACh transporter in some brain areas (Aghourian et al., 2017).

618 Finally, cholinesterase inhibitors seem to have some favorable effect in the treatment of
619 Alzheimer's disease patients (Sharma, 2019).

620 It is unclear to what degree the amount of agonist liberated used iontophoretic application of
621 cholinergic agonists emulates a relevant physiological condition (Minces et al., 2017). The
622 application of exogenous ACh, as we used here, could potentially surpass physiological
623 concentrations, making the results hard to extrapolate to a behaving animal. Furthermore,
624 future studies should investigate the effects of different doses of ACh on auditory processing
625 to determine if there is a dose-response relationship as well as the effect of muscarinic- and
626 nicotinic receptors blockade to theoretically observe more akin, analogous physiologically
627 effects. Similarly, forthcoming studies using optogenetic techniques to activate only basal
628 forebrain cholinergic neurons while also recording from auditory cortex neurons, will allow a
629 fine-grained investigation of the role of cortical acetylcholine on sensory representation.
630 Moreover, because our study was carried out in anaesthetized animals, it precludes
631 generalization of the effects of ACh on behaving states (Quintela-Vega et al., 2023). Future
632 studies using an awake preparation will confirm a definitive corroboration of the effect of
633 ACh on precision and determine the behavioral relevance of these findings.
634

635 The available neurobiological evidence suggests that precision is encoded by the synaptic
636 gain of superficial pyramidal cells encoding prediction errors, which are controlled by
637 neuromodulatory systems (e.g., dopaminergic, cholinergic) and/or synchronized neural
638 activity (Feldman and Friston, 2010; Kok et al., 2012b). However, we do not find changes in
639 prediction error precision in the superficial layers; our analysis suggests instead that the
640 effects of ACh were more limited to the deep AC layers (Fig. 8e). We observed a distinct and
641 differential distribution of units throughout the cortical layers, contingent upon the influence
642 of ACh on their selectivity index (SI). Units exhibiting an SI decrease during ACh application

were predominantly located and biased in layers III-IV and its adjacent regions, while those demonstrating an SI increment during ACh application spanned from the deeper layer IV to layer VI (Fig. 10b). In the initial conceptualizations of predictive coding, it was posited that prediction units reside in the infragranular layers (layers V and VI), with error units situated in supragranular layers (layers I – III) (Bastos et al., 2012; Friston, 2005). Alternatively, some models suggest that error units would be localized in the granular layer (layer IV), while prediction units would be detected in both supra- and infragranular layers (biased competition model of predictive coding; Spratling, 2008). In our recordings, units displaying an SI reduction during ACh application were also those with a higher SI under baseline conditions (i.e., larger response to deviant than to standard stimuli), thereby potentially qualifying as error units. These units were identified in layer IV and neighboring areas, which appears to support the model proposed by Spratling (2008). Furthermore, according to Eggermann and Feldmeyer (2009), the application of ACh would filter weak sensory inputs to layer IV and amplify signals at superficial and deep layers, effectively increasing the signal to noise ratio. In contrast, units demonstrating an SI increase during ACh application could be considered potential prediction units; such units were detected in granular and deep layers but were absent in superficial layers. This observation aligns with both predictive coding models, as each postulate that deep layers contain prediction units. A very interesting study would have been to estimate whether the neurons we record from were excitatory or inhibitory based on the spike shape. Indeed, we have previously shown that both types of responses show prediction error (Pérez-Gonzalez et al., 2021) but ACh may affect them differentially and this potential divergence may explain some of the variance of the data. This would involve implementing a similar analysis as done in our previous study (Pérez-Gonzalez et al., 2021), however that study used single-unit recordings and here we used multi-unit recordings. In the present data the recordings captured occasional spikes from other neurons which introduced

668 alterations in the average spike shape, and thus precluded an accurate categorization.
669 Therefore, we decided to discard this analysis for the sake of accuracy and appropriate
670 scrutiny awaits future studies.

671 In conclusion, we have shown that ACh plays a multifold role in modulating nMM in AC,
672 affecting the precision of prediction error signaling and gating prediction errors to
673 hierarchically higher processing levels.

674

675 **MATERIALS AND METHODS**

676 **Subjects and surgical procedures**

677 The experimental protocols were approved conforming to the University of Salamanca
678 Animal Care Committee standards and the European Union (Directive 2010/63/EU) for the
679 use of animals in neuroscience research. Experiments were performed on 37 adult female
680 Long-Evans rats with body weights within 180-250 g. We used female rats as our previous
681 work are based on this sex but no attempt to study gender dimension was aimed, which would
682 have required a larger number of animals. Surgical anesthesia was induced and maintained
683 with urethane (1.5 g/kg, intraperitoneal), with supplementary doses (0.5 g/kg, intraperitoneal)
684 given as needed. Dexamethasone (0.25 mg/kg) and atropine sulfate (0.1 mg/kg) were
685 administered at the beginning of the surgery to reduce brain edema and the viscosity of
686 bronchial secretions, respectively. Normal hearing was verified with auditory brainstem
687 responses (ABR) recorded with subcutaneous needle electrodes, using a RZ6 Multi I/O
688 Processor (Tucker-Davis Technologies, TDT) and processed with BioSig software (TDT).
689 ABR stimuli consisted of 100 µs clicks at a 21/s rate, delivered monaurally to the right ear in
690 10 dB steps, from 10 to 90 decibels of sound pressure level (dB SPL), using a closed-field
691 speaker. After the animal reached a surgical plane of anesthesia, the trachea was cannulated

692 for artificial ventilation and a cisternal drain was introduced to prevent brain hernia and brain
693 edema. Isotonic glucosaline solution was administered periodically (5–10 ml every 7 h,
694 subcutaneous) throughout the experiment to prevent dehydration. Body temperature was
695 monitored with a rectal probe thermometer and maintained between 37 and 38°C with a
696 homeothermic blanket system.

697 The auditory cortex surgery was described in previous works (Nieto-Diego and Malmierca,
698 2016; Parras et al., 2017) . The temporal bone was exposed and the auditory cortex was
699 located using stereotactic coordinates (Paxinos et al., 1997). A craniotomy was performed
700 over the auditory cortex, the dura was removed carefully, and the exposed area was filled with
701 a layer of agar to prevent desiccation and to stabilize the recordings. Before applying the agar,
702 a magnified picture (25×) of the exposed cortex was taken with a digital camera coupled to
703 the surgical microscope (Zeiss) through a lens adapter (TTI Medical). The picture included a
704 pair of reference points previously marked on the dorsal ridge of the temporal bone, indicating
705 the absolute scale and position of the image with respect to bregma (the reference point). This
706 picture was displayed on a computer screen and was overlapped with a micrometric grid, over
707 which the placement of the multibarrel for every recording was marked. The micrometric grid
708 allowed the generation of coordinates in a two-dimensional axis, from the superimposed
709 image of the auditory cortex of each animal. Once the coordinates of each of the recorded
710 units of all the animals were obtained, we used the functions 'griddata' and 'contourf' of
711 MATLAB to generate topographic maps (through a graduation of colors) of the characteristic
712 frequency (CF), Common SSA Index (CSI) levels, and deviant and standard tone responses in
713 all auditory cortical fields.

714 **Electrophysiological recording and microiontophoresis**

715 A tungsten electrode (1–3 MΩ) was used to record multiunit neuronal activity. It was attached
716 to a 5-barrel multibarrel borosilicate glass pipette that carried drug solution to be delivered in
717 the vicinity of the recorded neuron. The multibarrel's tip was cut to a diameter of 20-30 µm.
718 The center barrel was filled with saline solution for current compensation (165 mM NaCl)
719 whereas the others barrels were filled with 1 M acetylcholine chloride (Sigma, catalog no.
720 A6625). The pH was adjusted between 4.0-4.2 (Ayala and Malmierca, 2015). Drugs were
721 retained by applying a -15 nA current, and were ejected when required, typically using 30–40
722 nA currents (Neurophore BH-2 System, Harvard Apparatus). The duration of the drug
723 ejection usually lasted 8–10 min and the recording protocols were extended until the effect of
724 the drug had disappeared (60 to 90 minutes approx.). The multibarrel assembly was
725 positioned over the pial surface of the auditory cortex, forming a 30° angle with the horizontal
726 plane towards the rostral direction, and advanced using a piezoelectric micromanipulator
727 (Sensapex) until we observed a strong spiking activity synchronized with the train of search
728 stimuli made of white noise. Analog signals were digitalized with a RZ6 Multi I/O Processor,
729 a RA16PA Medusa Preamplifier and a ZC16 headstage (TDT) at 12 kHz sampling rate and
730 amplified 251x. Neurophysiological signals for multiunit activity were band-pass filtered
731 between 0.5 and 4.5 kHz.

732 **Experimental Design and stimulation paradigms**

733 Sound stimuli were generated using the RZ6 Multi I/O Processor (TDT) and custom software
734 programmed with the OpenEx Suite (TDT) and MATLAB. Sounds were presented
735 monaurally through a speaker, in a closed-field condition to the ear contralateral to the left
736 auditory cortex. We calibrated the speaker to ensure a flat spectrum up to ~75 dB SPL
737 between 0.5 and 44 kHz; the second and third harmonics were at least 40 dB lower than the
738 fundamental at the loudest output level for all the frequencies. The experimental stimuli were
739 pure tones in the range 0.5–44 kHz, with a duration of 75 ms, including 5 ms rise/fall ramps

740 presented at a rate of 4 stimuli/s. Once a suitable neuron was found, the frequency response
741 area (FRA) of the cell, i.e. the combination of frequencies and intensities capable of evoking a
742 suprathreshold response, was obtained automatically using a randomized paradigm that
743 presented tones between 0.5-44 kHz in 25 logarithmic steps, with intensities spaced by 10 dB
744 steps, from 0 to 70 dB SPL, at a repetition rate of 4/s. Based on this information, we selected a
745 pair of frequencies evoking similar responses at 10–30 dB above threshold. We used pure
746 tones at these frequencies as the stimuli in the oddball paradigm. Oddball sequences consisted
747 of frequently repeating stimuli (standard tones) which were pseudo-randomly interleaved with
748 rare events (deviant tones). Two oddball sequences with fixed parameters (400 trials each, 75
749 ms stimulus duration, 0.5 octaves frequency separation, 10% deviant probability, 250 ms
750 onset to onset, and a minimum of three standard tones before a deviant) were presented for
751 every pair of stimuli thus selected. In one of the sequences, the low frequency (*f1*) was the
752 "standard" and the high frequency (*f2*) was the "deviant," and in the other sequence their roles
753 were inverted. The order of presentation of these two sequences was randomized across sites.
754 In some cases, one or more extra pairs of stimuli were selected, and the oddball sequences
755 were repeated with the new stimuli.

756 According to the predictive coding framework, mismatch responses like those obtained during
757 an oddball paradigm can be divided in two components: repetition suppression, a reduction in
758 the response caused by a repeated stimulus, and prediction error, an increased response caused
759 by the violation of a regularity (Carbajal and Malmierca, 2018). In a subset of the
760 experiments, we used control sequences to evaluate the separate contribution of repetition
761 suppression and prediction error. Control sequences consisted of 10 tones evenly spaced by
762 0.5 octaves (same as in the oddball sequences), including the tones used in the oddball
763 paradigm, and all stimuli at the same previously chosen sound level. Each control sequence
764 lasted 400 trials, the duration of all stimuli was 75 ms and the presentation rate 4/s. We used

two different control sequences, namely the many-standards and cascade sequences (Supplementary Figure 1). The many-standards control is the consecutive presentation of blocks of 10 tones randomly ordered within the block, each tone with a 10% probability of occurrence (Schroger and Wolff, 1996). In this sequence the tones are unpredictable, and it is not possible to establish a rule which could be used to predict the following tones. On the other hand, the cascade control consists of the regular presentation of the same 10 tones in ascending or descending frequency succession (Ruhnau et al., 2012). This sequence also avoids the effects of the repetition of a single stimulus, but in this case, it maintains a predictable context. Cascade sequences are considered a more rigorous control than many-standard sequences because like the oddball sequence, a regularity is established (Carbajal and Malmierca, 2018).

**Data analysis**

We calculated the bandwidth of the FRAs (Fig. 4) for each recorded unit by measuring the width of the response area in octaves (relative to the low frequency border), at 10 and 30 dB above minimum threshold (BW10 and BW30, respectively).

The degree of nMM was quantified by the common SSA index (CSI), reported previously (Malmierca et al., 2009; Ulanovsky et al., 2004, 2003). The CSI reflects the difference between the neural responses to the deviant and standard stimuli, normalized to the total of responses to both stimuli, and is defined as:

$$CSI = \frac{d(f_1) + d(f_2) - s(f_1) - s(f_2)}{d(f_1) + d(f_2) + s(f_1) + s(f_2)}$$

where $d(f_i)$ and $s(f_i)$ are responses to each frequency $f_1$ or $f_2$ when they were the deviant ($d$) or standard ($s$) stimulus in the oddball paradigm, respectively.

Similarly, a frequency-specific SSA index (SI) was calculated for each of the frequencies presented in an oddball paradigm, as:

$$SI = \frac{d(f) - s(f)}{d(f) + s(f)}$$

Where *d(f)* and *s(f)* are responses to frequency *f* when it was the deviant (*d*) or standard (*s*) stimulus in the oddball paradigm, respectively.

For the subset of experiments where we recorded the many-standards and cascade controls, we compared the responses to the same physical stimulus when it took the role of a standard, a deviant (ascending or descending, depending on whether the preceding standard was of lower or higher frequency, respectively), or was part of a cascade sequence (matching the ascending or descending condition of the corresponding deviant). Alongside the oddball paradigm, we recorded responses of neurons to two cascade sequences (ascending and descending), which consisted of 10 tones selected within the FRA presented in a predictable succession of increasing or decreasing frequencies. We did not include the many-standards control in these analyses because these experiments are time-consuming and the need of holding the recording neuron for long enough before, during and after the drug injection. However, we have previously demonstrated that the many-standards and cascade controls responses were comparable, and the latter is considered to be more rigorous. (Casado-Román et al., 2019; Parras et al., 2017; Ruhnau et al., 2012; Valdés-Baizabal et al., 2019).

The responses of each neuron were normalized for each tested frequency as

$$Normalized\ Deviant = Deviant/N$$

$$Normalized\ Standard = Standard/N$$

$$Normalized\ Control = Control/N$$

where

$$N = \sqrt{Deviant^2 + Standard^2 + Control^2}$$

is the Euclidean norm of the vector defined by the deviant, standard and cascade responses, so that the normalized responses take values in the range 0–1.

With these normalized baseline-corrected spike counts, we next computed the indices of neuronal mismatch (iMM), repetition suppression (iRS), and prediction error (iPE) as:

$$iMM = Normalized\ Deviant - Normalized\ Standard$$

$$iRS = Normalized\ Control - Normalized\ Standard$$

$$iPE = Normalized\ Deviant - Normalized\ Control$$

Index values ranged between -1 and 1 and facilitated the quantitative decomposition of neuronal mismatch into repetition suppression and prediction error since

$$iMM = iRS + iPE$$

Which is largely comparable to the CSI calculated for the oddball paradigm (Parras et al., 2017). In order to determine a significant effect of the drugs on the CSI (Fig. 5a), we calculated an empirical distribution of CSI values by performing 2000 bootstraps of the responses to each standard or deviant stimulus for each neuron in the control condition, from which we determined a 95% confidence interval (vertical lines in Fig. 5a). An effect was considered significant at $\alpha$=0.05 if the CSI during the drug condition fell beyond the limits of the control CSI confidence interval (red dots in Fig. 5a). An equivalent approach was followed for the SI values in Fig. 6a.

The area under the receiver operating characteristic (ROC) curve (AUC) was calculated using the firing rates in response to deviant or standard stimuli as predictors (Figs 5d and 6c,d).

Mutual Information of the firing rates in response to deviant or standard stimuli was calculated using the Information Breakdown Toolbox (Magri et al., 2009).

The confidence intervals for the variance of the different index distributions (Fig. 8), were obtained by performing 1000 bootstraps.

Since parameters did not follow a normal distribution, non-parametric statistics were used: Mann-Whitney (for independent data) or Wilcoxon Signed Rank test (for paired data). Multiple comparisons were corrected using the Holm-Bonferroni approach. Unless stated otherwise, all data are reported as mean ± SD. All of the data analyses were performed with Sigma Plot v12.5 and MATLAB software, using the built-in functions, the Statistics and Machine Learning toolbox, or custom scripts and functions developed in our laboratory.

**Acknowledgments**: We thank Drs. Francisco Garcia-Rosales and Julio Hechavarria for their advice in the mutual information analysis and Drs. Ryszard Auksztulewicz, Yaneri A. Ayala, Donald Caspary, Diego Contreras, Karl Friston, Lauren Harms and Marina Picciotto for their constructive criticisms on a previous version. Finantial support was provided by the Spanish Agencia Estatal de Investigación grant (AEI), PID2019-104570RB-I00 (MSM, ABLR); the European Union's Horizon 2020 grant agreement No 952378- BrainTwin (MSM, DPG, ABLR) and the Foundation Ramón Areces grant CIVP20A6616 (MSM and DPG).

**Competing interests**: No competing interests declared

## REFERENCES


Aghourian M, Legault-Denis C, Soucy J-P, Rosa-Neto P, Gauthier S, Kostikov A, et al. 2017. Quantification of brain cholinergic denervation in Alzheimer's disease using PET imaging with [18F]-FEOBV. *Mol. Psychiatry* **22:**1531–1538. doi: 10.1038/mp.2017.183

Auksztulewicz R, Friston K. 2016. Repetition suppression and its contextual determinants in predictive coding. *Cortex* **80**:125–140. doi:10.1016/j.cortex.2015.11.024

Auksztulewicz R, Friston KJ, Nobre AC. 2017. Task relevance modulates the behavioural and neural effects of sensory predictions. *PLoS Biol* **15**:e2003143. doi:10.1371/journal.pbio.2003143

Auksztulewicz R, Rajendran VG, Peng F, Schnupp JWH, Harper NS. 2023. Omission responses in local field potentials in rat auditory cortex. *BMC Biol* **21**:130. doi:10.1186/s12915-023-01592-4

Auksztulewicz R, Schwiedrzik CM, Thesen T, Doyle W, Devinsky O, Nobre AC, Schroeder CE, Friston KJ, Melloni L. 2018. Not All Predictions Are Equal: "What" and "When" Predictions Modulate Activity in Auditory Cortex through Different Mechanisms. *J Neurosci* **38**:8680–8693. doi:10.1523/JNEUROSCI.0369-18.2018

Ayala YA, Malmierca MS. 2015. Cholinergic Modulation of Stimulus-Specific Adaptation in the Inferior Colliculus. *J Neurosci* **35**:12261–12272. doi:10.1523/JNEUROSCI.0909-15.2015

Bastos AM, Usrey WM, Adams RA, Mangun GR, Fries P, Friston KJ. 2012. Canonical Microcircuits for Predictive Coding. *Neuron* **76**:695–711. doi:10.1016/j.neuron.2012.10.038

Batista-Brito R, Zagha E, Ratliff JM, Vinck M. 2018. Modulation of cortical circuits by top-down processing and arousal state in health and disease. *Curr Opin Neurobiol* **52**:172–181. doi:10.1016/j.conb.2018.06.008

Carbajal G V., Malmierca MS. 2020. Novelty Processing in the Auditory System: Detection, Adaptation or Expectation? In: Fritzsch B, Gothe B, editors. The Senses: A Comprehensive Reference. Elsevier. pp. 749–776. doi:10.1016/B978-0-12-809324-5.24154-0

Carbajal G V., Malmierca MS. 2018. The Neuronal Basis of Predictive Coding Along the Auditory Pathway: From the Subcortical Roots to Cortical Deviance Detection. *Trends Hear* **22**:233121651878482. doi:10.1177/2331216518784822

Casado-Román L, Carbajal G V., Pérez-González D, Malmierca MS. 2020. Prediction error signaling explains neuronal mismatch responses in the medial prefrontal cortex. *PLoS Biol* **18**:e3001019. doi:10.1371/journal.pbio.3001019

Casado-Román L, Pérez-González D, Malmierca MS. 2019. Prediction errors explain mismatch signals of neurons in the medial prefrontal cortex. *bioRxiv* 778928. doi:10.1101/778928

Chavez C, Zaborszky L. 2017. Basal forebrain cholinergic-auditory cortical network: Primary versus nonprimary auditory cortical areas. *Cereb Cortex* **27**:2335–2347. doi:10.1093/cercor/bhw091

Chen I-W, Helmchen F, Lütcke H. 2015. Specific Early and Late Oddball-Evoked Responses in Excitatory and Inhibitory Neurons of Mouse Auditory Cortex. *Soc Neurosci*. doi:10.1523/JNEUROSCI.2240-15.2015

Colangelo C, Shichkova P, Keller D, Markram H, Ramaswamy S. 2019. Cellular,

Synaptic and Network Effects of Acetylcholine in the Neocortex. *Front Neural Circuits* **13**:24. doi:10.3389/fncir.2019.00024

Dalley JW, Cardinal RN, Robbins TW. 2004. Prefrontal executive and cognitive functions in rodents: neural and neurochemical substrates. *Neurosci Biobehav Rev* **28**:771–784. doi:10.1016/j.neubiorev.2004.09.006

Dasgupta R, Seibt F, Beierlein M. 2018. Synaptic release of acetylcholine rapidly suppresses cortical activity by recruiting muscarinic receptors in layer 4. *J Neurosci* **38**:5338–5350. doi:10.1523/JNEUROSCI.0566-18.2018

Edeline JM. 2012. Beyond traditional approaches to understand the functional role of neuromodulators in sensory cortices. *Front Behav Neurosci* **6**:1–14. doi:10.3389/fnbeh.2012.00045

Eggermann E, Feldmeyer D. 2009. Cholinergic filtering in the recurrent excitatory microcircuit of cortical layer 4. *Proc Natl Acad Sci U S A* **106**:11753–11758. doi:10.1073/pnas.0810062106

Feldman H, Friston KJ. 2010. Attention, Uncertainty, and Free-Energy. *Front Hum Neurosci* **4**:215. doi:10.3389/fnhum.2010.00215

Felix RA 2nd, Chavez VA, Novicio DM, Morley BJ, Portfors CV. 2019. Nicotinic acetylcholine receptor subunit $\alpha_7$-knockout mice exhibit degraded auditory temporal processing. *J Neurophysiol.* 122(2):451-465. doi: 10.1152/jn.00170.2019

Franklin NT, Frank MJ. 2015. A cholinergic feedback circuit to regulate striatal population uncertainty and optimize reinforcement learning. *Elife* **4**:1–29. doi:10.7554/eLife.12029

Friston K. 2023. Computational psychiatry: from synapses to sentience. *Mol Psychiatry* **28**:256–268. doi:10.1038/s41380-022-01743-z

Friston K. 2018. Does predictive coding have a future? *Nat Neurosci* **21**:1019–1021. doi:10.1038/s41593-018-0200-7

Friston K. 2008. Hierarchical Models in the Brain. *Cit Frist K* **4**:1000211. doi:10.1371/journal.pcbi.1000211

Friston K, Kiebel S. 2009. Cortical circuits for perceptual inference. *Neural Networks* **22**:1093–1104. doi:10.1016/j.neunet.2009.07.023

Friston KJ. 2005. A theory of cortical responses. *Philos Trans R Soc B Biol Sci* **360**:815–836. doi:10.1098/rstb.2005.1622

Froemke RC, Merzenich MM, Schreiner CE. 2007. A synaptic memory trace for cortical receptive field plasticity. *Nature* **450**:425–429. doi:10.1038/nature06289

Fu Y, Tucciarone JM, Espinosa JS, Sheng N, Darcy DP, Nicoll RA, Huang ZJ, Stryker MP. 2014. A cortical circuit for gain control by behavioral state. *Cell* **156**:1139–1152. doi:10.1016/j.cell.2014.01.050

Games KD, Winer JA. 1988. Layer V in rat auditory cortex: Projections to the inferior colliculus and contralateral cortex. *Hear Res* **34**:1–25. doi:10.1016/0378-5955(88)90047-0

Hampel H, Mesulam M-M, Cuello AC, Khachaturian AS, Vergallo A, Farlow MR, et al. 2018. Revisiting the Cholinergic Hypothesis in Alzheimer's Disease: emerging Evidence from Translational and Clinical Research. *J. Prev. Alzheimers Dis.* **6:**1–14. doi:10.14283/jpad.2018.43

Harms L, Parras GG, Michie PT, Malmierca MS. 2020. The Role of Glutamate Neurotransmission in Mismatch Negativity (MMN), A Measure of Auditory Synaptic Plasticity and Change-detection. *Neuroscience*. doi:10.1016/j.neuroscience.2020.01.046

Hasselmo ME. 1999. Neuromodulation: Acetylcholine and memory consolidation. *Trends Cogn Sci*. doi:10.1016/S1364-6613(99)01365-0

Hasselmo ME, Giocomo LM. 2006. Cholinergic Modulation of Cortical Function. *J Mol Neurosci* **30**:133–136. doi:10.1385/JMN:30:1:133

Hasselmo ME, Sarter M. 2011. Modes and models of forebrain cholinergic neuromodulation of cognition. *Neuropsychopharmacology*. doi:10.1038/npp.2010.104

Irvine DRF. 2018a. Auditory perceptual learning and changes in the conceptualization of auditory cortex. *Hear Res*. doi:10.1016/j.heares.2018.03.011

Irvine DRF. 2018b. Plasticity in the auditory system. *Hear Res*. doi:10.1016/j.heares.2017.10.011

Ishishita Y, Kunii N, Shimada S, Ibayashi K, Tada M, Kirihara K, Kawai K, Uka T, Kasai K, Saito N. 2019. Deviance detection is the dominant component of auditory contextual processing in the lateral superior temporal gyrus: A human ECoG study. *Hum Brain Mapp* **40**:1184–1194. doi:10.1002/hbm.24438

Kamke MR, Brown M, Irvine DRF. 2005. Basal forebrain cholinergic input is not essential for lesion-induced plasticity in mature auditory cortex. *Neuron* **48**:675–686. doi:10.1016/j.neuron.2005.09.014

Keller GB, Mrsic-Flogel TD. 2018. Predictive Processing: A Canonical Cortical Computation. *Neuron* **100**:424–435. doi:10.1016/j.neuron.2018.10.003

Kilgard MP, Merzenich MM. 1998. Cortical Map Reorganization Enabled by Nucleus Basalis Activity. *Science (80- )* **279**:1714–1718. doi:10.1126/science.279.5357.1714

Kok P, Jehee JFM, de Lange FP. 2012a. Less Is More: Expectation Sharpens Representations in the Primary Visual Cortex. *Neuron* **75**:265–270. doi:10.1016/j.neuron.2012.04.034

Kok P, Rahnev D, Jehee JFM, Lau HC, de Lange FP. 2012b. Attention Reverses the Effect of Prediction in Silencing Sensory Signals. *Cereb Cortex* **22**:2197–2206. doi:10.1093/cercor/bhr310

Lao-Rodríguez AB, Przewrocki K, Pérez-González D, Alishbayli A, Yilmaz E, Malmierca MS, Englitz B. 2023. Neuronal responses to omitted tones in the auditory brain: A neuronal correlate for predictive coding. *Sci Adv* **9**:eabq8657. doi:10.1126/sciadv.abq8657

Lucas-Meunier E, Fossier P, Baux G, Amar M. 2003. Cholinergic modulation of the cortical neuronal network. *Pflugers Arch* **446**:17–29. doi:10.1007/s00424-002-0999-2

Ma X, Suga N. 2005. Long-term cortical plasticity evoked by electric stimulation and acetylcholine applied to the auditory cortex. *Proc Natl Acad Sci U S A* **102**:9335–9340. doi:10.1073/pnas.0503851102

Magri C, Whittingstall K, Singh V, Logothetis NK, Panzeri S. 2009. A toolbox for the fast information analysis of multiple-site LFP , EEG and spike train recordings. *BMC Neurosci* **10**. doi:10.1186/1471-2202-10-81

Malmierca MS. 2015. Auditory System In: Paxinos G, editor. The Rat Nervous System. Elsevier - Academic Press. pp. 865–946.

Malmierca MS, Cristaudo S, Pérez-González D, Covey E. 2009. Stimulus-specific adaptation in the inferior colliculus of the anesthetized rat. *J Neurosci* **29**:5483–5493. doi:10.1523/JNEUROSCI.4153-08.2009

Marshall L, Mathys C, Ruge D, de Berker AO, Dayan P, Stephan KE, Bestmann S. 2016. Pharmacological Fingerprints of Contextual Uncertainty. *PLoS Biol* **14**. doi:10.1371/journal.pbio.1002575

Martins ARO, Froemke RC. 2015. Coordinated forms of noradrenergic plasticity in the locus coeruleus and primary auditory cortex. *Nat Neurosci* **18**:1483–1492.

doi:10.1038/nn.4090
Mesulam M-M. 2013. Cholinergic circuitry of the human nucleus basalis and its fate in Alzheimer's disease. *J Comp Neurol* **521**:4124–4144. doi:10.1002/cne.23415
Metherate R. 2011. Functional connectivity and cholinergic modulation in auditory cortex. *Neurosci Biobehav Rev* **35**:2058–2063. doi:10.1016/j.neubiorev.2010.11.010
Metherate R, Cox CL, Ashe JH. 1992. Cellular bases of neocortical activation: Modulation of neural oscillations by the nucleus basalis and endogenous acetylcholine. *J Neurosci* **12**:4701–4711. doi:10.1523/jneurosci.12-12-04701.1992
Minces V, Pinto L, Dan Y, Chiba AA. 2017. Cholinergic shaping of neural correlations. *Proc Natl Acad Sci U S A* **114**:5725–5730. doi:10.1073/pnas.1621493114
Moore DR. 2006. Auditory processing disorder (APD)-potential contribution of mouse research. *Brain Res.* 1091:200–206
Moore DR. 2012. Listening difficulties in children: bottom-up and top-down contributions. *J Commun Disord.* 45:411–418
Moran RJ, Campo P, Symmonds M, Stephan KE, Dolan RJ, Friston KJ. 2013. Free energy, precision and learning: The role of cholinergic neuromodulation. *J Neurosci* **33**:8227–8236. doi:10.1523/JNEUROSCI.4255-12.2013
Motts SD, Schofield BR. 2009. Sources of cholinergic input to the inferior colliculus. *Neuroscience* **160**:103–114. doi:10.1016/j.neuroscience.2009.02.036
Muñoz W, Rudy B. 2014. Spatiotemporal specificity in cholinergic control of neocortical function. *Curr Opin Neurobiol* **26**:149–160. doi:10.1016/j.conb.2014.02.015
Nelken I. 2014. Stimulus-specific adaptation and deviance detection in the auditory system: experiments and models. *Biol Cybern*. doi:10.1007/s00422-014-0585-7
Netser S, Zahar Y, Gutfreund Y. 2011. Stimulus-specific adaptation: Can it be a neural correlate of behavioral habituation? *J Neurosci* **31**:17811–17820. doi:10.1523/JNEUROSCI.4790-11.2011
Nieto-Diego J, Malmierca MS. 2016. Topographic Distribution of Stimulus-Specific Adaptation across Auditory Cortical Fields in the Anesthetized Rat. *PLoS Biol* **14**:1–30. doi:10.1371/journal.pbio.1002397
Ogawa H, Oka K. 2015. Direction-Specific Adaptation in Neuronal and Behavioral Responses of an Insect Mechanosensory System. *Soc Neurosci*. doi:10.1523/JNEUROSCI.1378-15.2015
Parr T, Friston KJ. 2017. Uncertainty, epistemics and active inference. *J R Soc Interface* **14**:20170376. doi:10.1098/rsif.2017.0376
Parras GG, Nieto-Diego J, Carbajal G V., Valdés-Baizabal C, Escera C, Malmierca MS. 2017. Neurons along the auditory pathway exhibit a hierarchical organization of prediction error. *Nat Commun* **8**. doi:10.1038/s41467-017-02038-6
Parras GG, Valdés-Baizabal C, Harms L, Michie PT, Malmierca MS. 2020. The effect of NMDA-R antagonist, MK-801, on neuronal mismatch along the rat auditory thalamocortical pathway. *Sci Rep* **10**:12391. doi:10.1038/s41598-020-68837-y
Pérez-González D, Parras GG, Morado-Díaz CJ, Aedo-Sánchez C, Carbajal GV, Malmierca MS. 2021. Deviance detection in physiologically identified cell types in the rat auditory cortex. *Hear Res.* **399**:107997. doi: 10.1016/j.heares.2020.107997
Pérez-González D, Schreiner TG, Llano DA and Malmierca MS. 2022. Alzheimer's Disease, Hearing Loss, and Deviance Detection. *Front. Neurosci.* **16**:879480. doi: 10.3389/fnins.2022.879480
Paxinos G, Watson C, Diego S, Boston L, York N. 1997. The Rat Brainin Stereotaxic Coordinates Academic Press.

Picciotto MR, Higley MJ, Mineur YS. 2012. Acetylcholine as a Neuromodulator: Cholinergic Signaling Shapes Nervous System Function and Behavior. *Neuron* **76**:116–129. doi:10.1016/j.neuron.2012.08.036

Pinto L, Goard MJ, Estandian D, Xu M, Kwan AC, Lee SH, Harrison TC, Feng G, Dan Y. 2013. Fast modulation of visual perception by basal forebrain cholinergic neurons. *Nat Neurosci* **16**:1857–1863. doi:10.1038/nn.3552

Polack PO, Friedman J, Golshani P. 2013. Cellular mechanisms of brain state-dependent gain modulation in visual cortex. *Nat Neurosci* **16**:1331–1339. doi:10.1038/nn.3464

Polley DB, Read HL, Storace DA, Merzenich MM. 2007. Multiparametric auditory receptive field organization across five cortical fields in the albino rat. *J Neurophysiol* **97**:3621–3638. doi:10.1152/jn.01298.2006

Puckett AC, Pandya PK, Moucha R, Dai W, Kilgard MP. 2007. Plasticity in the Rat Posterior Auditory Field Following Nucleus Basalis Stimulation. *J Neurophysiol* **98**:253–265. doi:10.1152/jn.01309.2006

Qi G, Feldmeyer D. 2022. Cell-Type Specific Neuromodulation of Excitatory and Inhibitory Neurons via Muscarinic Acetylcholine Receptors in Layer 4 of Rat Barrel Cortex. *Front Neural Circuits* **16**:1–16. doi:10.3389/fncir.2022.843025

Quintela-Vega L, Morado-Díaz CJ, Terreros G, Sánchez JS, Pérez-González D & Malmierca MS. 2023. Novelty detection in an auditory oddball task on freely moving rats. *Comms Biol.* doi:10.1038/s42003-023-05403-y.

Ruhnau P, Herrmann B, Schröger E. 2012. Finding the right control: The mismatch negativity under investigation. *Clin Neurophysiol* **123**:507–512. doi:10.1016/j.clinph.2011.07.035

Sarter M, Givens B, Bruno JP. 2001. The cognitive neuroscience of sustained attention: Where top-down meets bottom-up. *Brain Res Rev*. doi:10.1016/S0165-0173(01)00044-3

Schöbi D, Homberg F, Frässle S, Endepols H, Moran RJ, Friston KJ, Tittgemeyer M, Heinzle J, Stephan KE. 2021. Model-based prediction of muscarinic receptor function from auditory mismatch negativity responses. *Neuroimage* **237**. doi:10.1016/j.neuroimage.2021.118096

Schroger E, Wolff C. 1996. Mismatch response of the human brain to changes in sound location. *Neuroreport* **7**:3005–3008.

Sharma K. 2019. Cholinesterase inhibitors as Alzheimer's therapeutics. *Mol. Med. Rep.* **20:**1479–1487. doi:10.3892/mmr.2019.1 0374

Shipp S. 2016. Neural elements for predictive coding. *Front Psychol* **7**:1792. doi:10.3389/fpsyg.2016.01792

Spratling MW. 2008. Reconciling predictive coding and biased competition models of cortical function. *Front Comput Neurosci* **2**:4. doi:10.3389/neuro.10.004.2008

Timme NM, Lapish C. 2018. A Tutorial for Information Theory in Neuroscience. *eNeuro.* **5**(3):ENEURO.0052-18.2018. doi:10.1523/ENEURO.0052-18.2018.

Thiele A, Bellgrove MA. 2018. Neuromodulation of Attention. *Neuron*. doi:10.1016/j.neuron.2018.01.008

Ulanovsky N, Las L, Farkas D, Nelken I. 2004. Multiple time scales of adaptation in auditory cortex neurons. *J Neurosci* **24**:10440–10453.

Ulanovsky N, Las L, Nelken I. 2003. Processing of low-probability sounds by cortical neurons. *Nat Neurosci* **6**:391–398. doi:10.1038/nn1032

Valdés-Baizabal C, Carbajal G V., Pérez-González D, Malmierca MS. 2019. Dopamine gates prediction error forwarding in the cortices of the inferior colliculus. *bioRxiv* 824656. doi:10.1101/824656

von der Behrens W, Bäuerle P, Kössl M, Gaese BH. 2009. Correlating stimulus-specific adaptation of cortical neurons and local field potentials in the awake rat. *J Neurosci* **29**:13837–13849. doi:10.1523/JNEUROSCI.3475-09.2009

Vossel S, Weidner R, Driver J, Friston KJ, Fink GR. 2012. Deconstructing the architecture of dorsal and ventral attention systems with dynamic causal modeling. *J Neurosci* **32**:10637–10648. doi:10.1523/JNEUROSCI.0414-12.2012

Weinberger NM. 2004. Specific long-term memory traces in primary auditory cortex. *Nat Rev Neurosci* **5**:279–290. doi:10.1038/nrn1366

Yarden TS, Mizrahi A, Nelken I. 2022. Context-Dependent Inhibitory Control of Stimulus-Specific Adaptation. *J Neurosci* **42**:4629–4651. doi:10.1523/JNEUROSCI.0988-21.2022

Yon D, Frith CD. 2021. Precision and the Bayesian brain. *Curr Biol* **31**:R1026–R1032. doi:10.1016/j.cub.2021.07.044

Yu AJ, Dayan P. 2005. Uncertainty, Neuromodulation, and Attention. *Neuron* **46**:681–692. doi:10.1016/j.neuron.2005.04.026

Yu AJ, Dayan P. 2002. Acetylcholine in cortical inference. *Neural Networks* **15**:719–730. doi:10.1016/S0893-6080(02)00058-8

Zaborszky L, Hoemke L, Mohlberg H, Schleicher A, Amunts K, Zilles K. 2008. Stereotaxic probabilistic maps of the magnocellular cell groups in human basal forebrain. *Neuroimage* **42**:1127–1141. doi:10.1016/j.neuroimage.2008.05.055

1127 **SUPPLEMENTARY FIGURES**

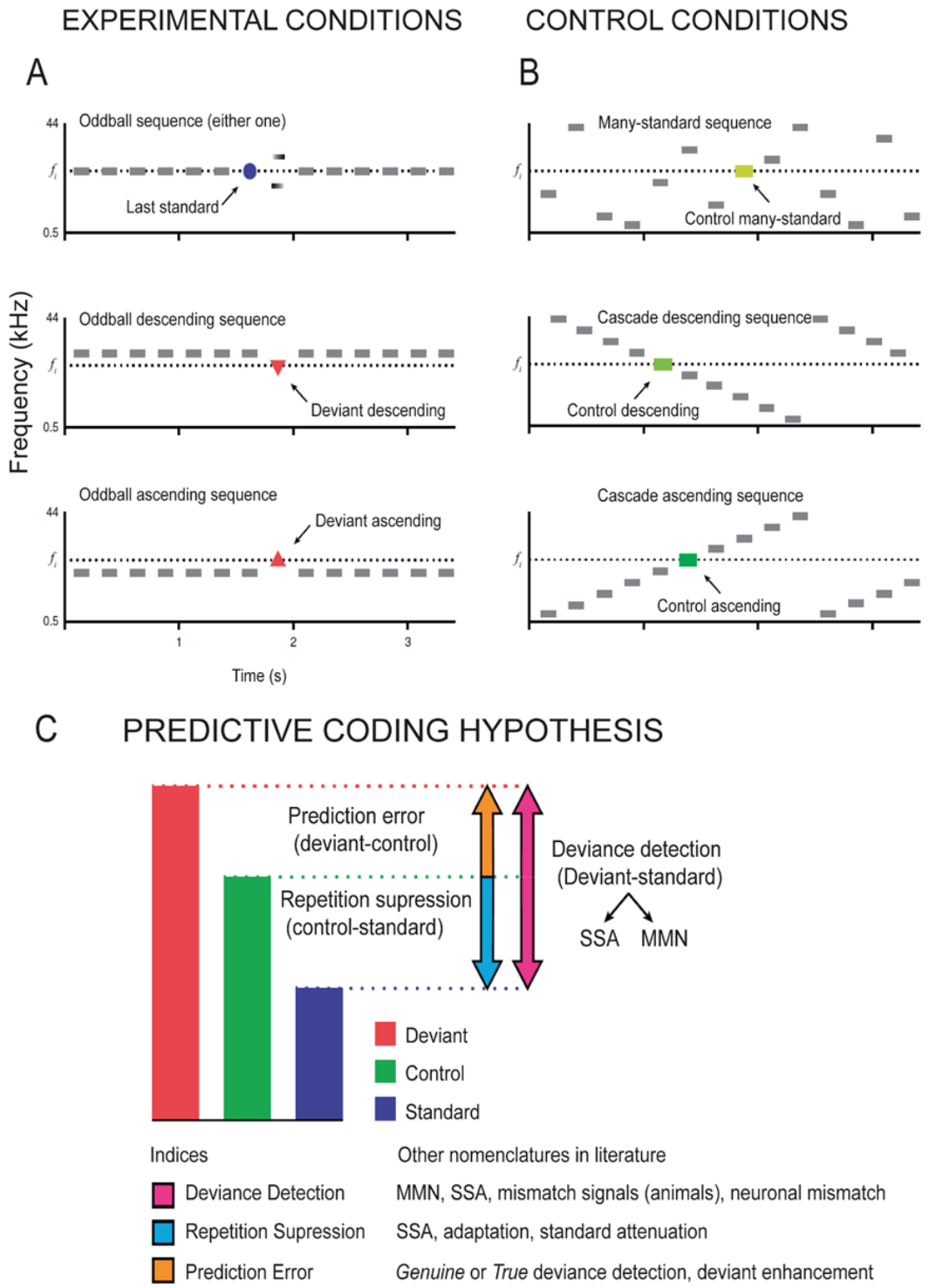


1128
1129 ***Supplementary Figure 1. Experimental paradigms and Interpretation of***

1130 ***the control conditions. (A)*** *Classic oddball paradigm, showing three*

1131 *possible experimental conditions for a given $f_i$ target tone: STD (blue circle,*

*top panel), DEV descending (red triangle pointing downwards, middle panel) and DEV ascending (red triangle pointing upwards, bottom panel).* ***(B)*** *CTR sequences highlighting the $f_i$ target tone. In the many-standard control (very light green rectangle), the target tone is embedded within a random succession of equiprobable tones, making it impossible for the system to establish a precise prediction or accurately encode a regularity. Two versions of the cascade sequence: Cascade descending sequence (light green rectangle) and Cascade ascending sequence (dark green rectangle) are compared with the DEV descending and ascending, respectively. In both versions, the target tone $f_i$ is embedded in a regular succession of equiprobable tones in both cases. This allows the system to generate a precise prediction or encode that regularity, because it is not violated by the appearance of the target tone $f_i$, as opposed to DEV.* ***(C)*** *Decomposition of the differential response by means of the control condition (green bar), yielding indices of mismatch (iMM, in magenta), prediction error (iPE, in orange) and repetition suppression (iRS, in cyan). Modified after Carbajal and Malmierca* (2020, 2018).